NTNU – Trondheim
Norwegian University of
Science and Technology

Investigation of Multi-degradation Mechanisms in Different Stainless Steels in Direct Riser Tensioning Systems for Offshore Oil&Gas Industry

Maciej Wladyslaw Andrzejewski

Master's Thesis
Submission date: June 2015
Supervisor: Nuria Espallargas, IPM
Co-supervisor: Amin Hossein Zavieh, IPM

Norwegian University of Science and Technology
Department of Engineering Design and Materials

Acknowledgments

The present project was conducted at Norwegian University of Science and Technology in Trondheim as a part of my student exchange.

I would like to express my gratitude to my supervisor and co-supervisor, Nuria Espallargas and Amin Hossein Zavieh, for their contribution to this project, especially for their guidance and willingness to shear their knowledge and experience.

I would also like to thank my family for all the support they gave me.

Abstract

Many components utilized in offshore industry are complex tribological systems, for instance Direct Riser Tensioner (DRT) cylinders which include the use of seals, guide bands, hydraulic fluids/lubricants and materials in relative movement. However, those components are often load bearing elements and thus fail due to the combined effect of multi-degradation processes (wear, corrosion and mechanical stresses). Moreover, the requirements for material selection and pre-qualification testing do not consider the synergy of the degradation phenomena, which leads to inaccurate evaluations and results in much shorter component lifetime than expected. It is therefore of a great importance to explain what happens in a material during multi-degradation exposure and how particular factors influence such a system, with emphasis on bending conditions, to be able estimate lifetime of components more precisely, thus diminish cost of maintenance and increase safe operation.

During experimental work two materials were tested: AISI 316L austenitic stainless steel (UNS S31603) and 25% Cr super duplex stainless steel (UNS S32750). Test were carried out at the multi-degradation test rig (LSMD) developed by NOV in cooperation with the Tribology research group at NTNU. Both environment related (normal and applied sustained/cyclic load, exposure time) and samples related (different materials and thus microstructure, grain size etc.) variables were changed and the effects were studied. Experiments were performed at OCP (with reference to Ag/AgCl reference electrode) in 3.4 wt% NaCl solution during reciprocating ball-on-plate sliding contact (∅4.76 mm alumina ball). Simultaneously either static or cyclic 4-point bending was applied and results compared to tribocorrosion exposure (also performed during tests).

The tests showed that tensile stresses from 4-point bending applied to a tribocorrosion system affect its volume loss and subsurface microstructure transformations. The effect on subsurface microstructure: tensile stresses release some fraction of compressive stresses induced by sliding contact, enlarge energy dissipation zone, and thus provide less subsurface deformations. Volume loss is affected as well - tensile stresses influence oxide kinetics growth on metal surface. The thickness of such surface film determines the size of debris particles generated during rubbing, and thus the volume loss.

Abstrakt

Mange komponenter som brukes i offshoreindustrien er komplekse tribological systemer, for eksempel Direct Riser Tensioner (DRT) sylindere som inkluderer bruk av sel, guide band, hydrauliske væsker / smøremidler og materialer i relativ bevegelse. Disse komponenter er ofte lastbærende elementer og kan på grunn av den kombinerte effekten av multi-nedbrytningsprosesser (slitasje, korrosjon og mekaniske påkjenninger) føre til brudd. Dessuten gjør kravene til materialvalg og pre-kvalifisering testing anser ikke synergien av nedbrytningsfenomener, noe som fører til unøyaktige evalueringer og resulterer i mye kortere levetid enn forventet. Det er derfor av stor betydning å forklare hva som skjer i et materiale under multi-nedbrytning eksponering. I denne masteroppgaven er det lagt vekt på bøyeforholdene, for å kunne estimere levetiden til komponenter mer presist, og dermed redusere kostnadene ved vedlikehold og øke sikker drift.

Under eksperimente ble to materialer testet: AISI 316L austenittisk rustfritt stål (UNS S31603) og 25% Cr super dupleks rustfritt stål (UNS S32750). Testen ble utført ved multi-nedbrytning testrigg (LSMD) utviklet i samarbeid med Tribology forskergruppe ved NTNU. Både miljørelaterte (normal og anvendt vedvarende / syklisk belastning, eksponeringstid) og eksempler relatert (forskjellige materialer og dermed mikrostruktur, kornstørrelse etc.) variabler ble endret og effektene ble studert. Forsøk ble utført ved OCP (med referanse til Ag / AgCl referanseelektrode) på 3,4 vekt% NaCl-oppløsning i løpet av frem- og tilbakegående ball-on-plate glidekontakt (Ø4.76 mm aluminiumoksyd-ball). Samtidig ble enten statisk eller syklisk 4-punkts bøying brukt og resultatene sammenlignet med tribokorrosjon eksponering (også utført i løpet av testene).

Testene viste at strekkspenninger fra 4-punkts bøying brukt på et tribokorrosjon system påvirket volumtapet og transformasjoner under overflaten. Effekten på microstruktueren under overflaten: strekkspenninger slipper ut noen fraksjoner av trykkspenninger indusert av glidende kontakt, større energiavgivelse sone, og således gir mindre deformasjoner under overflaten. Volumtap påvirkes også - strekkspenninger påvirker oksid kinetikk vekst på metalloverflaten. Tykkelsen av overflatefilmen bestemmer størrelsen av rusk partikler generert under gnidning, og dermed volumtapet.

Contents

Figures and tables

Nomenclature

AC	Alternating Current
AFM	Atomic Force Microscopy
alumina	Al_2O_3
ASS	AISI 316L austenitic stainless steel (UNS S31603)
BOP	Blow Out Preventer
CE	Counter Electrode
CF	Corrosion fatigue
COF	Coefficient of friction
CS	Carbon Steel
DRT	Direct Riser Tensioner
FIB	Focused Ion Beam
FCC	Face-Centered Cubic
HVOF	High Velocity Oxygen Fuel
LSMD	Lab scale Multi degradation
LVDT	Linear Variable Differential Transformer
NOV	National Oilwell Varco Norway AS
OCP	Open Circuit potential
O&G	Oil&Gas
PEEK	Polyether ether ketone
PLC	Programmable Logic Controller
PRE_n	Pitting Resistance Equivalent number
RE	Reference Electrode
SCC	Stress Corrosion Cracking
SEM	Scanning Electron Microscopy
SDSS	25% Cr super duplex stainless steel (UNS S32750)
WE	Working Electrode
XPS	X-ray photoelectron spectroscopy

1. Introduction

1.1. Purpose and objectives

Main purpose of this master thesis was to investigate and understand the multi-degradation phenomena in stainless steels utilized in offshore O&G industry. The research was focused on three major degradation mechanisms occurring in such harsh environment: wear, corrosion and fatigue. Instead of considering the influence of each one of them solely on degradation enhancement, the work will rather paid attention to their synergistic action.

Main objectives to be reached through this master work were:

- ✓ better understanding of tribocorrosion phenomena and factors relevant to the process in offshore environment, also how it differs from the tribology/corrosion solely,
- ✓ introducing fatigue (cyclic or sustained load) to the system and understanding its synergy with tribocorrosion.

During experimental work two materials were tested: AISI 316L austenitic stainless steel (UNS S31603) and 25% Cr super duplex stainless steel (UNS S32750). Test were carried out at the multi-degradation test rig (LSMD) developed by NOV in cooperation with the Tribology research group at NTNU [48], and thus it was the main equipment used to reproduce complex conditions that offshore conditions are exposed to. Both environment related (normal and applied sustained/cyclic load, exposure time) and samples related (different materials and thus microstructure, grain size etc.) variables were changed and the effects were studied.

Samples tested in multi-degradation environment were characterized and studied thoroughly by means of optical and confocal microscopes, SEM, XPS, FIB etc. to measure the wear damage, hardness deviation and to obtain better understanding of the processes occurring in a material during exposure to multi-degradation.

Specific objectives of the work were:

- ✓ Acquiring necessary experience and expertise in the field of tribology and tribocorrosion
- ✓ Fundamental understanding of fatigue assisted tribocorrosion
- ✓ Understanding of the effect of different variables on multi-degradation phenomena

1.2. Background

Today many exploration wells are located at water depths of between 1500 and 3000 m, meaning equally long riser pipes have to be used. A drilling riser is fixed to the seabed, connecting the well to the drilling vessel acting as an extension of the drilling well from the seabed to the drilling vessel's drilfloor. Direct Riser Tensioning (DRT) systems, consist of 6 large hydraulic cylinders (with a stroke length of 16m) providing tensioning of the drilling riser while compensating for the drilling vessel heave movements. Direct Riser Tensioner (DRT) cylinders are complex tribological systems, which include the use of seals, guide bands, hydraulic fluids/lubricants and materials in relative movement. These components fail due to the combined effect of multi-degradation processes (wear, corrosion and mechanical stresses). The origins of these degradation mechanisms lie at the atomic level and cause enormous loses in revenues (more than USD 550 000 per one day of down time), safety consequences and potential environment impact.

Nowadays the requirements for material selection and pre-qualification testing do not consider the synergy of the degradation phenomena, which leads to inaccurate evaluations and results in much shorter component lifetime than expected [1]. Currently used corrosion and wear (considered separately) test are for instance: salt droplet test, particle abrasion tests, pin abrasion test and scratch test. Other test such as hardness tests, impact testing and (static/dynamic) bending testing are performed as well. Nevertheless, mentioned test techniques do not consider the synergistic effect of the main multi-degradation phenomena occurring in such harsh environment, which created a need for a model that would take into account all of them. Such a model was developed [2] and will be presented in another section of this work, yet it still needs further investigation, since the fundamental and detailed understanding of this process is still limited.

1.2.1. System description

As it was mentioned above, DRT system consists of 6 large hydraulic cylinders (fig. 1a) with a stroke length of 16 m and a piston outer diameter in the range of 190-230 mm [1], which results in a slender component. The drilling riser on one end is to vessel's drillfloor and on the other to the seabed (to the blow out preventer – BOP - actually), acting as an extension of the drilling well and facilitating control of the well during drilling. The outer diameter of such riser pipe is typically 762 mm (30 inch) [1], and length equals to water depths, so up to

3000 m. However for different kinds of heavy machinery it is not that inconvenient to replace some components periodically, for offshore structures, due to harsh conditions and often hard reachable locations, it is of great significance to avoid such replacements as much as possible. The DRT system is vital to ensure safe drilling on a drilling rig, thus it is important to ensure its proper and reliable operation.

The cylinders operate like enormous pre-loaded gas springs and are exposed to harsh environment. They operate in seawater splash zone or even are partly submerged in it, thus are in direct contact with corrosive media, especially pronounced is the influence of chlorides. They are also load-bearing elements subjected to static and cyclic tensile loading due to compressive spring characteristics and heave movements of vessel and riser. Such conditions result in large axial load variations, bending loads and contact stresses (between sealing elements and guide bands in the packing box). Moreover, since the cylinders are inclined compared to the riser, this orientation manifests itself in the self-weight influence on contact stresses.

The cylinders operate at mid-stroke to ensure the compensation of heave/tidal movements of vessel and riser. This area is exposed both to corrosive media such as seawater and to abrasion. The latter may result from hard particles, such as silica coming from the drilling fluid or cementing operations, embedded in softer sealing material or guide bands. Such particles generate two-body and three-body abrasion on the piston rod surface. The typical sealing system (so-called packing box, fig. 1b) contains guide bands, sealing elements and wiper rings. Sealing elements contain the pressurized hydraulic fluid within the packing box, guide bands are the lateral load-bearing elements, often made of composite materials to prevent metal vs. metal contact, wipe rings in turn prevent the penetration of contaminants into the system. All these elements are expected to provide leak free operation possibly minimum wear friction. Due to high hydraulic pressure inside the cylinder the sealing elements are pressed towards piston rod surface ensuring tight system (leak free) but also resulting in high contact stresses. An embedded particle generates higher (by several orders of magnitude) contact stresses when being embedded in sealing material and higher bending loads when being embedded in guide bands. The consequences are: material degradation, loss of leak free system, hydraulic fluid leakage, loss of hydraulic pressure, and environment pollution. In hydraulic pistons utilized in offshore structures, the mineral oil-based fluid is replaced with fire-resistant water glycol-based fluid, for safety measure. However, compared

to the former it exhibits lower viscosity and worse lubrication provided. Also, its viscosity is more strongly affected by temperature fluctuations and pressure peaks.

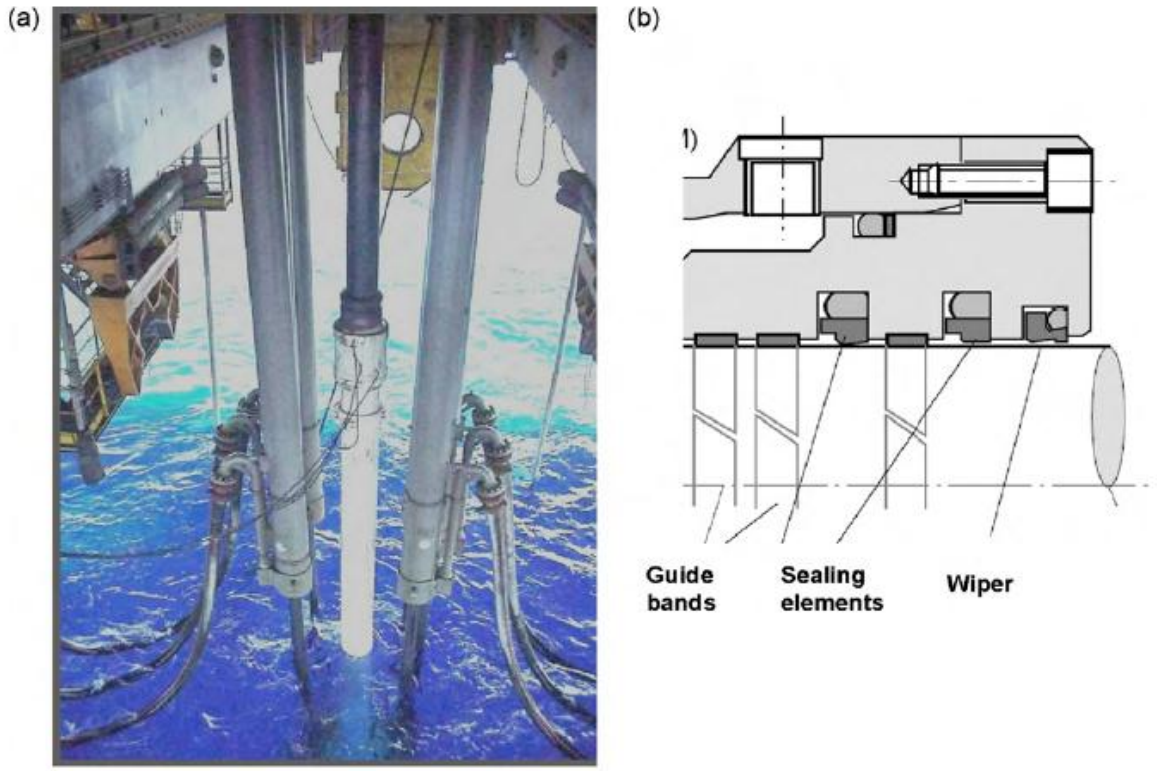

Fig. 1. (a) DRT cylinders with piston rods (b) simplified piston rod sealing system (packing box), left side: high pressure hydraulic fluid, right side: marine environment including seawater and particle pollution [2].

The surface properties of piston rod are a crucial factor in the talked-about system. It should be smooth (in order not to damage the sealing elements), hard (to withstand abrasive wear) and exhibit resistance to the surrounding environment – the corrosive media in this case. The cylinders operate mostly around mid-stroke, often with small amplitudes of the reciprocating movement. The amplitude depends on i.a. weather conditions: at calm weather the reciprocating movement is small, which can result in insufficient lubrication in the piston rod-sealing element interface; in case of storm in turn one should be concerned with extremely high loads rather than lubrication conditions.

The survey concerning premature failures of different DRT piston rods material combinations revealed following failures and their causes (by failure one assumed a major leakage resulted from sealing element damage or necessity of piston rod to be repaired in order to prevent such leakage) [3,4]:

- ✓ The operation time for plasma-sprayed ceramic coatings on carbon steel was less than 1 year; due to coating porosity and cracks seawater could penetrate through it and

cause the CS substrate corrosion, which resulted in coating blistering and delamination, and consequently sealing material damage (and hydraulic fluid leakage) due to sharp edges of the delaminated area,

- ✓ HVOF sprayed coatings on SDSS exhibited 2-3 years of operation time; degradation occurred due to mechanical and wear-induced failure mechanisms; the main factors were assumed to be: elastic properties, bond strength and corrosion of the coating,
- ✓ Uncoated SDSS piston rods exhibited the best resistance to such harsh conditions – no failures were noted; the material exhibited good corrosion resistance resulting from stable passive protective film of high integrity (even on the onset of rubbing); however, in the mid-stroke area the polishing effect were observed – such mechanism can lead to worse lubrication, and thus higher friction, which in turn can cause heat generation and consequently increased seal wear.

1.2.2. Literature overview

Multi-degradation of a material in marine environment is a complex phenomenon, which consists of many processes, that is why it is of great importance to get familiar with these processes and their principles while acting solely before proceeding to multi-degradation itself which involves simultaneous action of above mentioned, hence also a synergistic effect. In this section such different processes will be introduced, both while assuming their separate and simultaneous action.

1.2.2.1. Phenomena occurring during sliding of ductile materials

At first, let us consider sliding of material. We assume a ductile material, since the focus of this paper is the investigation of stainless steel behavior, and conditions of insufficient lubrication in order to focus on the material itself rather than on the influence of the surrounding environment meaning surface film, which will be considered in the next section.

During sliding a large plastic strain can be observed in the vicinity of sliding interface. The deformation extent depends on a few factors such as material, geometry and applied load and can vary from a few nm (for AFM contacts) to meters (while considering tectonic plates). Materials exhibit certain changes which let us assume that plastic flow is actually occurring. These are: changes in microstructure, marks/patterns on the surface and the rotation of

markers (artificially inserted or microstructure features allowing us to observe the changes, e.g. twins or conveniently oriented grain boundaries). Mentioned phenomena are usually investigated by means of precisely prepared cross-sections and let us observe that during sliding large plastic strains occur, also at large rates, moreover, the strain rates differ with the distance from the sliding interface.

Kuhlmann-Wilsdorf [5] and Hansen and Hughes [6] were investigating the deformation substructure of copper, which is of our interest since both copper and 316L stainless steel, as an austenitic steel, exhibit the same crystal system – FCC. In this case a relationship between strain/dislocation density and the dislocations arrangement emerges - the dislocations are spread randomly in form of tangles with no distinct pattern when the strain is low, whereas for higher strain rates the dislocations are organized into cell walls and subsequently create subgrain boundaries. This relationship has a pronounced influence on substructure grain size – in the latter case the grain size is much smaller than in the former. This phenomenon in turn influences microhardness of the material – the smaller substructure size, the higher the hardness – which refers to work hardening.

Material response becomes different in case of those with of more complex microstructure. An example can be a study carried out on Pb-Sn and Babbitt alloys [7] involving two of more phases, which reveals different behavior than copper. In vacuum or basically any chemically inert environment like mineral oil or inert gas, the material exhibits work softening. The reason for such behavior is a reduction in interface area in the microstructure, which is the basic driving force, as the lamellar structure in such alloy breaks down. However, the behavior is completely different as the environment changes to air. In such case work softening does not cover the whole material – close to the surface refined/fine-graded layer is created, which exhibits higher hardness than the bulk material.

Rigney et al. [8] was using X-ray diffraction and electron microscopy on transverse and longitudinal cross-sections of samples previously subjected to sliding contact. From the obtained results we can conclude that sliding influences the subsurface grain size and the crystallographic orientation, which is in agreement with previously mentioned studies stating the fact that as a result of sliding a refined subsurface layer is present.

As mentioned above, the material response can be completely different if we alter the microstructure - for example introduce a material with two or more phases. Moreover, if one of the phases is brittle it can cause failure by fracture, as it is possible for instance in pearlitic steel or aluminum reinforced with SiC particles. In the former case, during sliding with rolling

the carbides are rearranged and being oriented in sliding direction. Subsequently they fracture, which in turn favors the crack to propagate through softer ferrite [9]. The latter exhibits similar mechanism as well – SiC particles reinforce the base material providing reduced wear rate, however, above a critical load the particles fracture and their advantages are eliminated [10,11].

The change in subsurface grain size is not the only strain-induced phenomenon caused by sliding. The other example is phase transformation, which can occur in alloys with metastable structures such as austenitic stainless steels [12]. Depending on the chemical composition the stability for such steels varies and can lead to either strain-induced transformation or none transformation at all. The most stable of mentioned alloys is type 310 (1.7 Mn, 24.9 Cr, 20.2 Ni, 0.66 Si, all wt.%), type 316 (1.6 Mn,17.7 Cr, 13.8 Ni, 3.3 Mo, 0.4 Si, all wt.%) exhibits intermediate stability, whereas type 304 (1.6 Mn, 18.1 Cr, 8.3 Ni, 0.5 Si, all wt.%) easily undergoes transformation to martensite. What is interesting all these alloys exhibit similar sliding characteristics, but only for short sliding distances, otherwise they differ significantly.

When it comes to modeling the wear we meet an obstacle – since the gradient in grain size along the distance from the surface is present one cannot model the wear in terms of base material properties. In such case it is essential to estimate the location of maximum shear stress in terms of distance from the contact surface. It is known that the location of the maximum shear stress is below the surface for rolling or sliding with low friction, however, as the sliding friction coefficient rises and reaches the value of 0.3 the maximum shear stress is located at the surface. In the former case one should consider subsurface cracks, whereas in the latter one may assume that the cracks originate at the sliding surface. The problem here is that some cracks, which may seem to have origin subsurface, might in fact be an effect of lateral growth of a surface crack, grinding/polishing/etching or a presence of transfer material or some material with altered composition. To understand the latter further study of transfer and mixing is necessary.

In tribological interaction of two components a transition layer with a different composition from bulk material develops. Such layers are referred to as ‘third bodies’, which are described by Godet et al.[13] in the following manner: *“they flow and they transmit load, they separate or screen the ‘first bodies’, they accommodate velocity gradients, and they can be created, destroyed and regenerated during sliding. Their behavior depends on the dimensions, composition and properties, which may be close to material limits. They can be*

hard or soft and they can range from a single trapped particle to a continuous layer. The key distinguishing characteristic is chemical composition." There are two ways for new chemical elements to penetrate a tribological specimen: from the counter body and from the environment. Here emerges the significance of the environment, lubricant and subsequently surface film, which will be elaborated in the next section. Subsequently, the newly formed nanocrystalline layer [14] can be a mixture of different chemical compounds originating from either one of the first bodies or the environment. This indicates different microstructure of the nanocrystalline layer than the bulk material involving new phases. The proportion of each phase will affect mechanical properties of the material, as hardness, and subsequently also wear. One occurrence is very pronounced in such process – there is distinct and sharp boundary between the refined nanocrystalline layer and the rest of the material. It results from mechanical mixing where small volumes of material are transported by a flow process, with one remark – it takes place only to a certain depth from the surface and no further, hence the sharp boundary. Also, beneath the subsurface nanocrystalline layer a gradient structure is formed that separates the former and the bulk material, which will be described in next paraghaphs.

An interesting observation was made [15]: the debris particles generated during sliding have in most cases the exact structure and composition as the mixed layer of the base material. The subsequent conclusion is that debris is not generated directly from the base material. The mechanism is as following: during sliding local contacts cause plastic deformation and large plastic accumulation, which in turn favor shear instabilities in the subsurface layer of material. This facilitates transfer to happen and results in a layer of mechanically mixed material. The debris particles are generated then from this layer and its size determines the size of debris particles. One issue should me mentioned here: as a consequence of mentioned mechanical mixing and the fact that it occurs locally the properties of material – e.g. structure, hardness - can vary significantly throughout such mixed layer.

Returning to the subsurface layer, let us consider more thoroughly mechanisms occurring during its formation. A model of vertical motion was proposed [16] assuming "shear + rotation" motion of material volumes at mesoscale – 3D structural units called mesovolumes. During rubbing stress concentration exceeds yield strength, which after relaxation favors deformation, in this case rotational. Moreover, it was suggested that mass transfer occurs not only by dislocation slip but also by motion these mesovolumes. In such case the material in the subsurface layer exhibits a viscous paste behavior, which in turn

favors rotational plasticity. The slipping and rotation enables large friction-induced plastic strains in the subsurface layer, which results in opposite signs stains in the material beneath it. Eventually, as a result of this mechanism a gradient structure separating the subsurface nanocrystalline layer and the bulk material is developed. Returning to the rotational model – due to the surface not being ideally flat – its roughness and asperities – during sliding contact mechanical impacts between two surfaces' micropeaks occur generating stress waves – exponentially decaying – propagating into material [17]. This generates cracks and favors their propagation, within zones where stresses exceed yield strength, which in turn results in formation of layers with high defects density. The defects are organized in the manner of "dislocation walls" – low-angle misorientation boundaries [18], which enable the structure of the subsurface layer to be rearranged during the friction. Then a misfit develops between deformation in the refined subsurface layer and the lower layers with not deformed grains. Rotation of the mesovolumes with unequal grain sizes within allows generating new stress concentration locations. Shear is generated and simultaneous action of rotation and translation results in both compressive and tensile stresses, which favors formations of vortices at mesoscale.

1.2.2.2. Effect of surface films on the mechanical behavior of solid surfaces

It is well known that the environment, surface films in particular, has great impact on surface mechanical properties. It can alter ductility – Joffe effect [19] - or hardness by providing a surface hardening – Roscoe effect [20] - or softening – Rehbinder [21] and Kramer effect [22].

Kramer effect

Kramer described the mechanism responsible for altering mechanical properties of surface, the change in the work hardening rate in particular. He observed that the properties were changed by formation of new surface compounds. The phenomenon causing such effect was liberation of electrons (exoelectrones), which provided energy to the surface, necessary for the surface compound to develop. He attributed the liberation of the electrons to occurring deformation, however, as it was proven later by Ferrante [23] it resulted not from mechanical but from chemical interaction with the surface film. He investigated behavior of magnesium (both strained and annealed) in vacuum and observed that in such a clean state none of these

surfaces generates exoelectrons. However, after applying a small dose of oxygen liberation of the latter was observed. Further dose more caused increased exoelectrons emission, but another one caused quite opposite effect. It is explained by the oxygen layer that covered the surface after some time suppressing exoelectrons emission. Hence, Kramer observation was apt – the properties of a surface alter after formation of new surface compounds, however, the source of this formation are not exoelectrons (and their energy) liberated as a result of deformation, but chemical interaction between the surface and the environment – in this case oxygen adsorption, which actually liberates the exoelectrons.

Roscoe effect

Another pronounced effect of surface interaction with the environment is the Roscoe effect, which involves increase of surface hardness in the presence of oxide layer. It is observed in tribological systems in sliding, rolling and rubbing contact. Roscoe based his statement on observation of oxide layer on cadmium single crystals [20], however, the same effect was observed for gold covered by gold chloride layer [24]. Without the surface film the surface behaves in a ductile manner during sliding. The wear track is distinct and no other changes than plastic deformation are observed. In the presence of the surface film the mircohardness increases favoring different surface behavior. The surface film (oxide/chloride) suppresses plastic deformation and strain in sliding contact resulting such phenomena as twinning or even fracture, as the surface becomes more brittle after being hardened.

Joffe effect

The environment can affect also the ductility of the material. It can produce the surface softening effect and thus make the material less prone to brittle fracture (more ductile). The presence of surface active species can also reduce the formation and growth of fracture cracks as well as decrease the crack propagation velocity. It is a very important observation in terms of engineering purposes. For instance, oxygen was found to be very effective specie in terms of crack growth arrest in high strength steels in a hydrogen environment [25]. In hydrogen environment solely the crack length increases with time, however, by applying a small dose (0.6%) of oxygen the crack growth was completely was stopped after very short time. This effect applies also for other materials and environments, although the effect in general applies to aqueous environment.

Rehbinder effect

The effect is similar to the previous one. The difference is in the environment. Rehbinder was studying the influence of several organic acids on the surface properties of bunch of metals and nonmetals [21]. He observed increase in ductility and, what is important, in deformability of solid surfaces and decrease in hardness. He observed the surface absorbates reduce the shear strength of materials, both metals and nonmetals (including organic solids). This effect is not confined only to organic acids but applies also to other active liquids such as alcohols.

The above mentioned effect can affect different properties of a material. The Roscoe effect (material with a surface film - oxide layer) raises the stress-strain curve beyond the elastic limit, the Rehbinder effect (surface active liquid film) in turn lowers it. If a material surface exhibits all the three behaviors (including the normal one – dry sliding, for which the stress-strain curve lies between the one for Roscoe and Rehbinder effects) an appreciable difference in wear and friction characteristic is observed. The track width is widest for surface covered with active liquid and narrowest for oxidized one, the moderate one belongs to the dry one. The coefficient of friction exhibits the highest value for Rehbinder effect affected surface, because of weakened shear resistance at the interface.

1.2.2.3. Tribocorrosion – basis and mechanisms

In the following section basis and mechanism governing tribocorrosion system will be presented [26].

Tribocorrosion is a process of material degradation due to simultaneous action of wear and corrosion. It involves a mechanical action (sliding, fretting, rolling, impingement) in a corrosive environment. During such exposure the volume loss, which constitutes measure of material degradation, is often larger than the volume loss for corrosion and wear considered separately, which indicates the presence of a synergy effect. Of our interest is tribocorrosion of passive metals. On such metals a thin (1-10 nm) surface film is formed constituting a brrier against corrosion. In a tribocorrosion system the film rupture occurs exposing the bare material (depassivation) to anodic dissolution, which lasts until the passive film is re-built (repassivation).

Since tribocorrosion is a complex process it is not enough to consider each factor (wear and corrosion) solely to understand all the phenomena occurring in a tribocorrosion system. Several trials have been undertaken to explain the synergy of wear and corrosion in such a system. Each of those approaches depends on the background of the research group and the will be presented in next sections.

Before proceeding to tribocorrosion itself it seems appropriate to shed light on wear mechanisms in sliding contact and corrosion mechanisms in passive materials.

In the scope of this thesis we will confine our interest to sliding, since it is the most relevant case for in our case. Sliding is a relative motion of two surfaces in contact and can be either continuous or reciprocating. Two types of such contact are distinguished: two-body contact (when the sliding surfaces are in direct contact) and three-body contact (when the surfaces are separated by a lubricant, wear particles or deliberately added particles) and both of them can cause surface deterioration and wear in a tribocorrosion system. The term 'wear mechanisms in sliding contact' comprises such mechanisms as adhesive, abrasion, and fatigue wear.

- ✓ Adhesion occurs for two asperities in contact. In such case strong adhesive junctions might be formed and then broken by shearing stresses resulting from sliding motion. Subsequently one material is adhered to the other's surface. It may stay on the surface or leave the contact as a free particle.
- ✓ Abrasion is a case when one of the two surfaces in contact is significantly harder than the other one. It occurs as a result of hard asperities or a hard particle trapped between surfaces (which in turn can be a result of contamination or surface oxidation) – depending on which one is the case we distinguish two- and three-body abrasion, respectively.
- ✓ Fatigue results from continuous fluctuating loading and its symptoms are crack formation and, subsequently, flaking. Crack can initiate either on surface or subsurface and then propagate either to the interior of the material or up to the surface, respectively.

As to corrosion mechanisms in passive metals, the term comprises i.a.: depassivation, active dissolution, repassivation, passive dissolution, transpassive dissolution, adsorption and localized corrosion.

- ✓ When a counter body slides against surface, the surface film is being thinned or completely removed and thus exposing the bare material (depassivation), which results in its active dissolution. When having enough time the passive film is restored and the surface is repassivated until next counter body passage.
- ✓ Passive dissolution means formation of cations but at the metal-film interface. Those migrate then across the passive film to the film-electrolyte interface. Subsequently they dissolve in the solution. The prerequisite for this phenomenon to occur is nonzero solubility of metallic ions. However, the phenomenon in tribocorrosion system is neglected since it appears mainly outside the wear track and the corrosion rate of passive film dissolution is much lower than the corrosion rate of depassivated material within the wear track.
- ✓ When the passive film is oxidized to species with higher solubility we refer to it as transpassive dissolution.
- ✓ Adsorption occurs when the atoms at the surface exhibit unsaturated bonds, which can be fixed through reaction with atoms and molecules present in surrounding media, i.e. electrolyte. Adsorbed species may have influence on electrochemical processes (e.g. anodic dissolution, passive film formation) involved in corrosion.
- ✓ Localized corrosion is a selective process occurring on small areas and is favored by the presence of certain anions (e.g. chloride) in spots where the passive film is locally broken down.

Tribocorrosion has been approached from several different points of view trying to explain this complex phenomenon and these are presented below.

Synergistic approach

This approach originated from erosion-corrosion study and assumed the total material loss as a sum of individual contributions of corrosion and wear and the synergistic term. The former factors are determined in separate tests, which eliminate the mechanical part and the corrosion component (by applying a cathodic potential), respectively. The synergistic term involves the effect of simultaneous action of wear and corrosion: the change of corrosion due to wear (wear-accelerated corrosion, ΔC_w) and the change of wear due to corrosion (corrosion-

accelerated wear, ΔW_c). Subsequently, wear-corrosion maps were created to identify wastage regimes of materials in different electrolytes. They are determined as follows:

- ✓ Erosion dominated regime: $\Delta C_w / \Delta W_c < 0.1$
- ✓ Erosion-corrosion regime: $0.1 \leq \Delta C_w / \Delta W_c < 1$
- ✓ Corrosion-erosion regime: $1 \leq \Delta C_w / \Delta W_c < 10$
- ✓ Corrosion dominated regime: $\Delta C_w / \Delta W_c \geq 10$

This approach, formerly used in erosion-corrosion and abrasion-corrosion can be also applied to sliding systems of passive metals and coating. However, it is strongly dependent on the electrolyte used [27] and the applied cathodic protection potential [28].

Mechanistic approach

The mechanistic approach describes the total wear volume (V_t) as a sum of two factors: mechanical wear (V_{mech}) and metal loss due to chemical or electrochemical oxidation (V_{chem}). Strong dependence of one from another exists – anodic dissolution is affected by mechanical parameters and the mechanical material removal depends on prevailing electrochemical conditions. The total volume loss is described by following formula:

$$V_t = V_{mech} + V_{chem} \quad . \tag{1}$$

V_{chem} comprises the corrosion both in the passive area outside the wear track and in the depassivated area within the wear track. However, the former is negligible compared to the latter. This facilitates to determine the oxidation kinetics in situ and in real time by means of measuring the current flowing through the metal (I_p) in potentiostatically controlled experiment. In such case V_{chem} is obtained by using Faraday's law:

$$V_{chem} = {}^{QM}/_{nF\rho}\,, \tag{2}$$

where:

- ✓ Q – charge flowing in the wear track, obtained by integrating I_p over the time (t) of the experiment,
- ✓ M – atomic mass of the metal,
- ✓ n – apparent valence (the charge number for the oxidation reaction),
- ✓ F – Faraday's constant,
- ✓ ρ – density of the metal.

According to Landolt et al. in order to be able to apply eq.(2) two conditions must be met [29]:

- ✓ The cathodic partial current must be negligible meaning that the measured current equals the anodic partial current for metal oxidation,
- ✓ The charge number n for the metal oxidation reaction must be known.

Studies [29] have shown that the second term is of a great importance. It was observed that in the passive domain depending on the n value the chemical and mechanical contributions to the total wear differ significantly. However it can cause some inconveniences since for some pure metals the valence of the corrosion products varies with applied potentials and for alloys the chemical composition of oxides can be complex. Nevertheless, n can still be determined by means of very precise surface analysis – XPS (X-ray photoelectron spectroscopy).
The total wear volume is measured after the experiment by profilometric techniques, and subsequently the mechanical volume is obtained by subtracting from it the anodic volume.

The mechanistic approach has however its limitations. The two factors contributing to the total wear volume do not proceed independently, there is always some kind of interaction between them, thus this simple calculation of both of them cannot completely account for the whole process occurring in a tribocorrosion system, since it cannot explain phenomena such as e.g. build-up of third bodies.

Third body approach

This approach was based on the observation of wear debris formation during mechanical wear. In tribological contact the debris remains between surfaces for some amount of time before it is eliminated (removed, smeared back or oxidized) and before it happens it alters the wear rates by separating the wear surfaces and thus affecting the interaction between the first bodies. The metal volume loss (V_{met}) is describes by the following formula [26]:

$$V_{met} = V_{met}^{particle} + V_{met}^{ions} + V_{met}^{oxide}, \quad (3)$$

where:

- ✓ $V_{met}^{particle}$ – material removed due to abrasion, adhesion or delamination in form of solid particles,
- ✓ V_{met}^{ions} – material removed by dissolution (ions dissolved in the electrolyte),
- ✓ V_{met}^{oxide} – material oxidized to form the passive film.

Furthermore, the particles detached by means of mechanical interaction are subjected to some factors determining their final form. Total volume of mechanically removed particles is a sum of contributions of these factors, which describes eq. (4):

$$V_{met}^{particle} = V_{met,particle}^{ejected} + V_{met,particle}^{ions} + V_{met,particle}^{oxide} + V_{met,particle}^{smeared}, \quad (4)$$

where:

- ✓ $V_{met,particle}^{ejected}$ – volume of particles ejected from the contact,
- ✓ $V_{met,particle}^{ions}$, $V_{met,particle}^{oxide}$– volume of particles oxidized: dissolved in the electrolyte or forming the passive film, respectively,
- ✓ $V_{met,particle}^{smeared}$ – volume of particles being smeared back on the metal surface or transferred and smeared on the counter body surface.

The volume of wear track at the end of the experiment is expressed as follows:

$$V_t = V_{met} - V_{met,particle}^{smeared}, \quad (5)$$

which after substitution of eq.(3) and (4) yields:

$$V_t = V_{met,particle}^{ejected} + V_{met,particle}^{ions} + V_{met,particle}^{oxide} + V_{met}^{ions} + V_{met}^{oxide}. \quad (6)$$

The anodic volume (V_{chem}) can be introduced, with an assumption that metal and metal particles only oxidize electrochemically, i.e. in absence of oxidizing agents:

$$V_{chem} = V_{met,particle}^{ions} + V_{met,particle}^{oxide} + V_{met}^{ions} + V_{met}^{oxide}, \quad (7)$$

which after substitution to eq.(6) yields:

$$V_t = V_{met,particle}^{ejected} + V_{chem}. \quad (8)$$

Thus, the calculated mechanical wear (V_{mech}) amounts to the metal particles ejected from the contact, however, it one should keep in mind that it does not have to equal particles detached from the metal surface ($V_{met}^{particle}$), as it is explained above.

Three situations can be distinguished to interpret the tribocorrosion phenomena by means of the third body approach:

- ✓ $V_t = V_{mech} = V_{met}^{particle}$, meaning that the first as well as the third body does not undergo an anodic reaction and thus V_{mech} determines the total mechanical material removal from the first body.

- ✓ $V_{met,marticle}^{ions} = 0$, meaning that the first body is likely to oxidize/dissolve, but the third body is not, thus the mechanical wear rate is the difference of measured total wear V_t and the anodic wear V_{chem} determined by measured current and Faraday's law.
- ✓ $V_{met,particle}^{ejected} = 0$, meaning that all wear particles are either dissolved or transformed into oxide before leaving the contact, thus $V_{chem} = V_t$.

Moreover, the third body influence on the contact is pronounced as it can alter the conditions occurring either by acting as an abrasive and thus enhancing wear or by acting as a solid lubricant and decreasing friction and subsequently wear. Its behavior depends on a few parameters, such as:

- ✓ Mechanical parameters: contact pressure, lubrication, sliding velocity,
- ✓ Surface chemistry: metal oxidation and dissolution, adsorption from the environment
- ✓ Material properties: chemical composition, hardness, microstructure.

Examples of such dependence:

- ✓ the higher the normal load, the more wear debris is formed [30,31,32],
- ✓ much more debris is formed in materials with higher hardness [33] than in more ductile materials [34],
- ✓ at potential attributed to immune behavior of material, it deforms in totally plastic manner and thus the wear track surface is smooth, whereas in higher potential, when an oxide is formed, crack are observed as a result of brittle material behavior [35].

Nanochemical wear approach

During sliding (in both dry and lubricated conditions) a material undergoes surface deformation, which is a key factor determining its wear. The nanochemical wear approach is based on the assumption that friction and wear have some impact on the physical properties in tribocorrosion contact and on the mechanical properties of the subsurface. The approach assumes two steps:

- ✓ nanocrystalline structure is formed at the contact subsurface as a result of strain accumulation,
- ✓ nano-grains are then detached from the surface generating wear.

However, the exact mechanism is still not clear.

Basically, sliding is assumed to result in presence of three zones [36], starting from the surface as follows:

- ✓ mechanical mixed layer (zone 3): consists of material mixed from both the bulk and the counterpart, can be divided into two layers: tribochemical reaction layer and nanocrystalline mixed layer,
- ✓ plastically deformed layer (zone 2) – layer with a grain-size gradient, the grain size varies from highly strained nanocrystalls at the zone 2-zone 3 interface to low strained grains within the bulk material,
- ✓ bulk material (zone 1)

As was mentioned before, the boundary between the nanocrystalline mixed layer and the material underneath is observed to be very sharp and distinct. Also, the material exhibits different properties in zones 1 and 3. As a consequence of mechanical mixing and chemical changing in zone 3 one may expect work hardening of the surface. Moreover, due to altered crystalline structure the stress-strain response of the material within zone 3 can change, which may lead to change in parameters like: strain to failure, Young's modulus and the coefficient of friction.

The subsurface transformation is dependent on material properties and prevailing electrochemical conditions. Due to plastic deformation resulting from sliding dislocation formation and movement occurs, which may lead to mechanical milling and dynamic recrystallization. Dislocations form so called dislocation cells, which can be also a consequence of fatigue. The dislocation movement direction is towards the surface. At cathodic applied potential no surface film is formed thus the dislocations are annihilated at the surface. On the other hand, at passive applied potential the passive film is formed at the surface and acts as a barrier for dislocations annihilation and thus favors dynamic recrystallization. Consequently, the obtained refined layer (zone 3) thickness is bigger than in case of applied cathodic potential [37]. Finally this approach aims to account for the role of the nanocrystalline layer on the wear – it is expected that rather than delamination and fatigue, detachement of nanocrystalls during sliding occurs. In the study on this phenomenon [38] nano-abrasion marks and low wear coefficients independently on the material hardness were observed and attributed to nanochemical wear mechanism.

The study [37] of tribocorrosion behavior of 304L stainless steel/alumina contact in sulphuric acid in passive/cathodic conditions confirmed the above assumptions. The samples were characterized by means of SEM, FIB and EBSD techniques, so the ones used in this thesis as

well. Also, this study, due to similarity to our case – austenitic stainless steel with similar microstructure and mechanical properties, is worth taking a look at. Observations made and conclusions drawn are:

- ✓ since the average Hertzian pressure was much higher than the yield strength of the steel, plastic deformation was assumed to occur,
- ✓ as a consequence of metal subsurface deformation build-up of a highly deformed layer near the surface, which exhibits a gradient in grain size with size increasing across the depth,
- ✓ in general, the plastic deformation (originating from sliding action) alters the microstructure, within which three zones can be distinguished: undeformed bulk material (1), the plastic gradient layer (2) and mixed nanocrystalline layer (3) at the surface, sharp boundaries between those zones were noticed,
- ✓ the deformation, and thus the thickness of refined layer is highly dependent on the applied potential: at passive applied potential (meaning in a presence of oxide film formed at the surface) the grain refinement (and thus the deformed layer thickness) was more pronounced, as well as the defects density was higher, all in comparison to cathodic (no surface film) applied potential,
- ✓ the reason for such difference is greater strain accumulation in case of passive potential – the frictional shear stress (with maximum at the surface for COF < 0.3) generates dislocations, which can either diffuse inside the material towards the bulk of the steel or be annihilated at the surface; however, in the presence of surface film (at passive applied potential) the annihilation can be reduced or even completely blocked, which in turn favors the diffusion of the dislocations into the material and their higher density in the subsurface layer,
- ✓ defects observed were: vacancies, dislocations, interstitial atoms, twinning,
- ✓ the grain size was estimated to decrease exponentially with distance from the surface, which indicates exponentially decreasing strain in the same direction,
- ✓ the wear track surface was smoother for applied cathodic potential, it also contained less and smaller scratches, no alumina transfer to metal surface was observed,
- ✓ the surface work hardened during sliding contact, the effect is more pronounced for passive applied potential,
- ✓ the passive film thickness was observed to be independent from applied potential,

- ✓ the reduction in grain size, as well as martensite nanograins transformation from austenite in case of passive potential (higher strain accumulation), were attributed to dynamic recrystallization caused by large plastic strain,
- ✓ during rubbing the current increased as a result of increasing area exposed to anodic metal dissolution.

Since the thesis is focused on material behavior in marine environment, different factors affecting tribocorrosion in such conditions should be considered [39]:

- ✓ chloride content and dry/wet conditions: the chloride content (i.e. salinity) varies of the atmospheric conditions and geographical location, and so in the North Sea it equals 34‰, in the Caspian Sea 31‰, in the Malaysian and Indonesian water 32-33‰, in Brazil 37‰ and in the Gulf of Mexico 36‰; in general, the higher the salinity, the tougher are the conditions and the stronger corrosion attack; when a component is wetted only periodically, salt deposits may form at the surface, and due to high chloride content enhance material degradation,
- ✓ temperature and sun exposure: the temperature accelerates the degradation processes, thus the piston rods located in water at higher temperatures and more exposed to sunlight are more prone to undergo degradation, which is explained by the corrosion kinetics – with increasing temperature the rate of diffusion and electrochemical reactions at the interface increases,
- ✓ hydraulic fluid/ lubrication: the viscosity (and thus lubrication conditions) of the hydraulic fluid utilized in offshore hydraulic cylinders (mentioned earlier) alters depending on temperature; however, it affects not only lubrication itself – according to the theory stated in [3] the fluid of low viscosity can easily penetrate an open surface crack being trapped, and then be pressurized during crack closure resulting in 'wedging effect' and crack propagation,
- ✓ joint action of tribocorrosion and mechanical loading: as described in section 1.2.1; tensile stresses may generate micro-cracks in the coating, which allows the penetration of chloride containing seawater to the CS substrate and consequently its degradation by corrosion; subsequently these crack may propagate and cause coating delamination.

1.2.2.4. Influence of surface residual stresses and contact loads on surface wear

After considering the contribution of environment (electrolyte) and wear (sliding contact) both when acting separately and simultaneously it is time to move on to the material residual stresses and their influence on a tribocorrosion system.

The study [40] conducted on CoCrMo in air by means of AFM at different contact loads and residual stresses (compressive/tensile) led to some interesting conclusions. It was observed, that for higher average contact pressure a higher wear rate can be observed. Also, the stress state is of a great importance in terms of decreasing/enhancing wear rate: the presence of compressive stress increases wear rate whereas tensile stress decreases it. The wear rate did not depend on hardness, the material response was similar across the whole sample depth.

This approach assumes surface deterioration resulting from two processes: surface damage and repassivation. During sliding contact both the oxide film and the underlying substrate may be damaged, the proportion of this damage is determined by the residual stress within material. In case of oxide damage/removal the underlying material will immediately repassivate forming new oxide layer. Both processes are affected by prevailing stress state as follows:

- ✓ As to repassivation: residual stress influences the oxidation kinetics either by decreasing or enhancing passive film growth. Furthermore, surface stress state may alter the reaction kinetics, which can result in different repassivated layer composition, depending on the surface stress level. However, the exact nature of this phenomenon is still not clear due to its complex synergistic behavior.
- ✓ In case of surface damage, the oxide coated material can be considered two dissimilar elastic materials (the oxide layer and the underlying substrate) under a residual stress field [41]. When a crack reaches the interface between them it is expected to behave in one of three ways: it can cross the interface and dissipate the energy in the substrate; it can detach both materials by propagating along the interface; it can be arrested at the interface. The path that the crack follows depends on the stress state. In case of hard surface film covering a ductile material it is much more likely for a crack to penetrate the substrate if it is subjected to tensile stress than to compressive stress. Tensile stress favors more energy dissipation into substrate through plastic deformation and thus decreasing surface film damage [42]. Reversely, compressive stress hinders energy dissipation through substrate plastic deformation and thus results in more severe surface film damage than in case of tensile stress.

1.2.2.5. Multi-degradation model for passive metals exposed to seawater

In this section a multi-degradation model [2] for passive metals in seawater, assuming interaction between tribocorrosion and static/cyclic loading on surface, will be presented, as well as the first results of tests of such behavior in ASS and SDSS.

The purpose of this model is to describe influence of applied fatigue and tensile stresses in a tribocorrosion system. The model was assumed to be applied i.a. in DRT systems described in section 1.2.1. for large hydraulic piston rods. Its background and cause of its development was previously described in section 1.

The multi-degradation model is based on two issues. First one covers the question of fatigue in a corrosive environment. The interaction between those two factors is referred to as corrosion fatigue (CF) and stress corrosion cracking (SCC) mechanisms. Corrosion fatigue is basically material degradation under combined action of corrosion and cyclic loading. It exhibits a great significance to material behavior. The best example is the effect on S-N curves, which manifests itself in lowering the fatigue limit of a material in a corrosive environment in comparison to the ambient one. Other definition claims: "*Fatigue cracking in corrosive environment, or usually known as corrosion fatigue (CF), has been defined as the superposition of fatigue crack propagation in an inert environment and crack propagation under sustained load in a corrosive environment (so-called stress corrosion cracking (SCC)).*" [2]

Second issue involves tribocorrosion behavior and is based on models presented in section 1.2.2.3. The main aspects covered are:

- ✓ Corrosion degradation (V_c): pure corrosion without wear; dependent on i.a. passive current density and metal area exposed to anodic dissolution,
- ✓ Wear degradation including wear loss without corrosion in a reference environment (V_w) and material loss due to dry wear (V_{w0}); relevant factors are for the latter: normal contact force, surface hardness and sliding distance, and for the former: sliding frequency and time, crack growth rate in a reference environment (without corrosion); it is referred to as micro-fatigue wear, during which a laminar propagation of debris formation is assumed (parallel to the surface),
- ✓ Wear-accelerated corrosion (V_{wc}): it was found that the average anodic current measured during sliding depends on the real contact area (represented by normal force,

metal hardness, sliding distance and frequency) and the metallic dissolution charge [43]; however, it does not include two issues: effect of repassivation and dissolution of generated third-body particles in the electrolyte, and the current flow between active (worn) and passive (unworn) area, which cannot be detected by potentiostat; also, it was found that for a surface repassivating rapidly just a small fraction of the anodic current density accounts for metal dissolution [44,45,46],

- ✓ Corrosion-accelerated wear (V_{cw}): the concept is based on low-cycle micro-fatigue cracking (micro-fatigue) for generating wear debris particles in a corrosive environment, which includes: localized corrosion attack (e.g. micro-pitting) enhancing possibility of crack initiation and thus generation of micro-fatigue tribocorrosion debris particles; and dependence of above mechanism on "*the weakening of bonding or reduction of surface energy at the crack tip caused by embrittlement due to reactive species at the crack tip according to CF and SCC theories*" [2],

Below the multi-degradation model is presented. It assumes:

- ✓ Complementing the material loss due to pure wear with the effects of cyclic loading,
- ✓ adding the contribution of CF and SCC, which enhance corrosion-accelerated wear.

Conditions for the multi-degradation model

The multi-degradation model refers only to passive metals in contact with seawater, thus operating in conditions similar to the ones described in section 1.2.1. The model simulates a hard third-body particle being embedded in the sealing material and in the sliding contact with the passive metal, with simultaneous exposure of the metal surface to static/cyclic tensile loading originating from either axial tension or bending. For assumed case – passive metal operating in seawater – pitting and crevice corrosion should be studied most thoroughly. The multi-degradation model assumes two boundary conditions: the material hardness and corrosion resistance. Both are presented below.

The materials wear rate is often related to the normal load and hardness of the softest material in contact. In the model a two body contact between the metal surface and the abrasive particle is assumed. When the surface hardness ($HV_{surface}$) exceeds some specific value, a certain increase in the surface abrasive wear resistance is observed, moreover, there is also a value, above which the maximum wear resistance is achieved. Both values are experimentally determined and amount to 0.5 and 1.3 times the hardness of abrasive particle ($HV_{abrasive\ particle}$),

respectively. Assuming the abrasive particle as silica with hardness of 1260 HV [2] and knowing the hardness of stainless steels/coating used in offshore piston rods applications (250-350 HV for SDSS and 600-650 HV for 80Ni-20Cr HVOF coating [3,4]) the range of interest is the lower one in this case:

$$0.5\ HV_{\text{abrasive particle}} < HV_{\text{surface}} \quad (9)$$

The change in abrasive wear resistance is attributed to the level of plastic deformation on the material surface during sliding and how much contact pressures the particle can withstand without any deformation occurring.

In order to be able to qualitatively rank stainless steel alloys in terms of corrosion resistance, a specific value called pitting resistance equivalent (PRE_n) was introduced and described as follows:

$$PRE_n = \%Cr + 3.3(\%Mo + 0.5\%W) + 16\%N \quad (10)$$

The higher the PRE_n value, the more robust passive oxide layer on the stainless stesl is formed. It is known that for seawater environment PRE_n values higher than 40 provide a stable and high integrity passive protective film and thus sufficient corrosion resistance. Thus, based on the survey [3,4], it is reasonable to assume that above that value one can neglect the pure corrosion loss both outside the wear track and in the repassivated area inside the wear track. PRE_n values for SDSS and ASS equal 42.2 and 24, respectively.

In the multi-degradation model no presence of third-body particles rolling between interacting surfaces is assumed, or none third-body particles for that matter. The reason for this assumption is the set-up the system, which the model is designed for – the system operates both in vertical orientation and in seawater splash zone (or is totally submerged), thus all debris particles are immediately removed from the contact zone. As a consequence of such conditions no protective compacted layer is formed on the surface.

Finally, assuming a stable passive film (assessed as mentioned above) on the metal surface in seawater environment, the multi-degradation model predicts two possible operating conditions being dependent on the surface and abrasive particle hardness ratio. For that purpose eq.(9) is utilized and determines, whether the “pure” wear loss (without synergy enhancement) should be considered in the total degradation or not:

Degradation condition 1

$$HV_{surface} > 0.5\ HV_{abrasive\ particle} \quad (11)$$

For this condition the total material loss ($V_{t>0.5}$) is expressed by the following equation:

$$V_{t>0.5} = \Delta V = V_{wc} + V_{fw} + V_{cfw}\ , \quad (12)$$

where:

V_{wc} – wear-accelerated corrosion, meaning the material loss due to metal dissolution in the depassivated area,

V_{fw} – fatigue assisted wear, meaning the material loss due to joint action of tensile stress and micro-fatigue wear (in the same environment without corrosion),

V_{cfw} – corrosion- and fatigue-assisted wear, meaning the material loss of the combined interaction of CF, SCC and corrosion induced micro-fatigue wear.

Since the surface hardness and the corrosion resistance is assumed to be high, the degradation condition 1 consider the contributions of pure wear and corrosion (V_w and V_c, respectively) to be negligible and involves only pure synergistic effects of multi-degradation.

Degradation condition 2

$$HV_{surface} \leq 0.5\ HV_{abrasive\ particle} \quad (13)$$

The total material loss is governed by the equation:

$$V_{t\leq 0.5} = V_w + \Delta V = V_w + (V_{wc} + V_{fw} + V_{cfw})\ , \quad (14)$$

which consist of the same mechanisms as the degradation condition, except for the pure wear loss(V_w), which is taken into account because of the low surface hardness of the metal, and thus low abrasive wear resistance.

Let us now proceed and consider each contribution of above mentioned material total loss (eq. (12) and (14)):

- ✓ fatigue assisted micro-fatigue wear (V_{fw})

  This factor involves complementing the material loss by pure friction wear with the effect of fatigue. Both fatigue processes - plain fatigue by tensional loading and micro-fatigue wear caused by sliding - have similar crack initiation mechanisms: penetration of fatigue slip bands or defects in the surface, which result in generation of critical

micro-cracks. However, the propagation of the crack goes varies in both cases: for the former mechanism the crack propagates into the material perpendicular to the surface, whereas for the latter in a laminar manner parallel to the surface. In order to determine V_{fw}, the total crack growth rate (g_R) is decomposed into vectors representing crack growth rates for each process solely, and since both these vectors act perpendicularly to each other it amounts to:

$$|\overrightarrow{g_R}| = \sqrt{g_r^2 + g_{ra}^2} = g_R \quad (15)$$

where:

$g_r = (\frac{da}{dN})_r$ – low-cycle micro-fatigue crack growth rate during sliding wear action,

$g_{ra} = (\frac{da}{dN})_{ra}$ – plain fatigue crack growth rate.

The presence of plain fatigue results in larger debris particles and increased material loss in comparison to only tribocorrosion.

- ✓ micro-fatigue wear assisted by CF and SCC (V_{cfw})

This term complements the corrosion-accelerated wear (V_{cw}) with the effect of crack propagation due to CF and SCC. It is assumed that the crack tip is affected by the localized corrosion, which enhances the micro-fatigue cracking mechanism. Since there is more than one possible loading condition (sustained load vs. cyclic load), the total crack growth rate is determined for each one of them.

The total crack propagation due to plan fatigue assisted micro-fatigue wear:

$$|\overrightarrow{g_{CFS}}| = \sqrt{g_{cfs}^2 + g_{cfc}^2} = g_{CFS} \quad (16)$$

The combined crack growth due to SCC (sustained load in a corrosive environment) caused both by residual stresses resulting from applied tensile loading and stresses being a consequence of sliding wear:

$$|\overrightarrow{g_S}| = \sqrt{g_s^2 + g_{scc}^2} = g_S \quad (17)$$

where:

$g_{cfs} = (\frac{da}{dN})_{cfs}$ – low-cycle micro-fatigue crack growth rate in CF conditions,

$g_{cfc} = (\frac{da}{dN})_{cfc}$ – crack growth rate due to fatigue in CF,

$g_s = (\frac{da}{dN})_s$ – low-cycle micro-fatigue crack growth rate in SCC conditions,

$g_{scc} = (\frac{da}{dN})_{scc}$ crack growth rate due to fatigue in SCC conditions.

This case is analogical to the previous one: the cracks resulting from micro-fatigue wear (g_{cfs} and g_{scc}) propagate parallel to the surface, whereas the cracks resulting from the tensile and bending loads propagate perpendicular to the surface - transverse to the applied stress (g_{cfc} and g_{scc}). The former mechanism causes formation of debris particles by delamination.

Since the model is fairly recent, there are still some limitations concerning it. It is therefore impossible to assess it precisely e.g. due to lacking data and methods to estimate the parameters for crack growth calculations. However, some evaluation can be done at this point, for instance: increased sliding frequency causes higher wear-assisted corrosion. The effect is of a great significance, which can be assessed as follows:

- ✓ low frequency means more time for the chemical reactions to occur at the crack tip, which results in its blunting, which in turn decreases the stress intensity and consequently crack propagation; that manifests itself in larger wear particles formation,
- ✓ medium frequency is responsible for the highest synergistic material loss, since the crack opening time is most optimal for the chemical reactions to occur, hence the bonding at the crack tip is being weakened by hydrogen diffusion; that results in increasing crack growth in each cycle,
- ✓ at high frequency the time for reaction to occur is too short to affect the crack tip in any noticeable manner, however, the effect for multi-degradation may still be higher than for tribocorrosion.

First tests based on this model were performed on SDSS and ASS [47]. Test were carried out at applied 4-point bending (to ensure maximum tensile stresses in bigger volume than in case of 3-point bending) at both OCP and 0mV potentiostatic conditions. Some observation made and conclusion drawn:

At OCP:

- The passive film, which is ruptured upon applied sliding and bending, does not fully repassivate during rubbing; the complete repassivation occurs after unloading, SDSS exhibits better repassivation response than ASS,
- based on COF results (COF value drop during cycling loading, also more fluctuating than during static loading) indicates that some changes in wear behavior occurs,

caused by structural transformations affecting the shear resistance and wear mechanisms,

- for both materials the effect of anodic activation (represented by potential drop) is more pronounced when applying bending to the tribocorrosion system, than without it, which may indicate more extensive weakening of the passive film also outside the wear track,
- volume loss increases with increasing bending frequency,
- microhardness results indicate that the surface inside the wear track tends to work soften (in reference to tribocorrosion conditions) at low cyclic loading and work harden as the cyclic exposure increases; the microhardness inside the wear track is always higher than outside, which is attributed to work hardening caused by sliding contact with the alumina ball,

At fixed 0 mV potential:

- the current flowing through the active area increases with time, which is attributed to wear-accelerated corrosion – with time the volume loss is bigger, consequently the alumina ball is digging deeper increasing the area exposed to anodic dissolution,
- fatigue influence is very pronounced – the highest volume loss is obtained for the highest number of bending cycles (frequency),
- the volume loss is in general higher than for OCP measurements, which indicates pronounced effect of polarization conditions compared to tribocorrosion solely,

Furthermore:

- since both material exhibited similar wear track morphology (a bit smoother surface on SDSS samples), it was concluded that they undergo similar wear mechanisms – micro-ploughing and micro-fatigue, which manifest themselves in abrasive wear and plastic deformation in the form of longitudinal marks in the wear track,
- the alumina ball exhibited almost none damage, only metal transfer on its surface, thus no additional third-body wear resulting from alumina ball damage can be assumed,
- samples characterization by means of SEM revealed such features as: deformed and broken austenitic grains (SDSS, triboroccorion only), deformed austenite mixing with deformed ferrite (SDSS with applied cyclic loading), twins and slip bands (more visible at cyclic loading), refined subsurface layer that is much thicker for tibocorrosion than for static/cyclic loaded samples (ASS, OCP).

1.2.3. LSMD test rig

The purpose of development of this test rig was a need to simulate multi-degradation exposure conditions. This is obtained by introducing to the system multi-degradation processes:

- ✓ Friction wear by means of reciprocating rubbing of alumina ball against test sample (continuous contact of both is ensured by a dead weight hanging on a line and pressing one toward the other),
- ✓ Corrosion by means of corrosive media (electrolyte), which the sample in immersed in,
- ✓ Tensile stress – applied 4-point static/cyclic bending by means of reciprocating movement of rods applying bending force on the sample.

Simplified sketch of the test rig is depicted at fig. 2. The sketch represents one test chamber and the test rig consists of 6 of those. This allows to perform multi-degradation test either on samples of the same material at different combinations of multi-degradation conditions or on samples of different materials subjected to the same multi-degradation conditions.

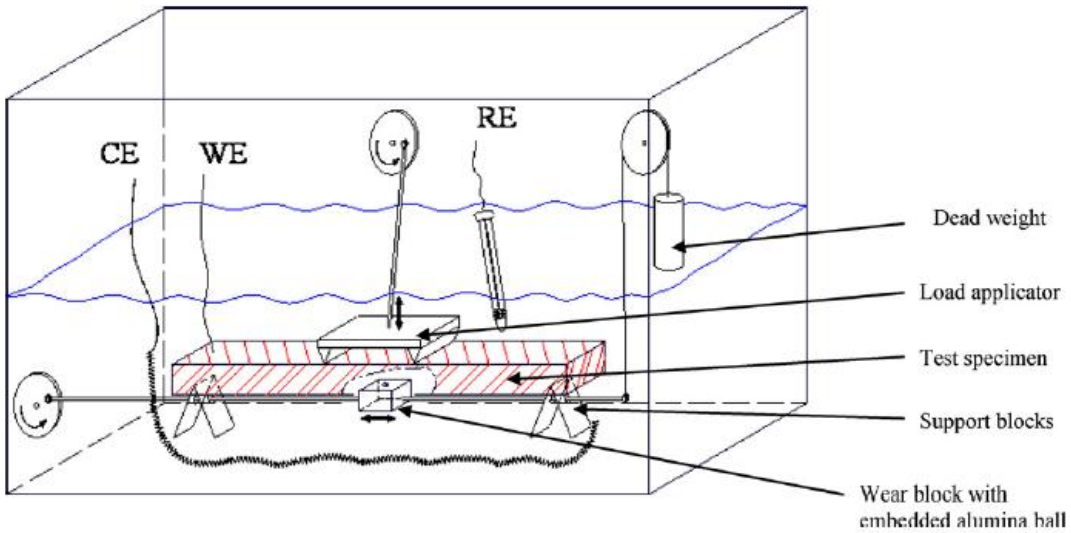

Fig. 2. Simplified sketch of the multi-degradation test rig [48].

Mechanical layout

The test sample rests on supports blocks fixed to the floor of test chambers (fig. 3b). The supports are rounded to allow sample to deform, and are made of PEEK to withstand

degradation in corrosive environment and to allow minimum deformation under applied loading. The load applicator (fig. 3b and d) is pushing down the sample applying the 4-point bending. It contacts the sample at two sites, which are 50 mm apart, and is free-floating so it can easily adjust its location to the sample surface. The purpose of such configuration and applying 4-point bending is to ensure maximum tensile stresses in the area between those two points. Thanks to that maximum stress at the whole wear track length is provided.

Torque is transmitted from the electric AC motor (mounted on the top of the test rig) via gear and transmission chain drive to the overhead shaft (fig. 3a), which rotate two eccentric wheels (cam discs). To this discs two rods are connected and by pushing/pulling provide linear reciprocating movement to dolly (rigid load beam), which is guided by guide rollers confined by the main frame. The dolly transfer the linear up/down motion to 6 rods, which induce the bending load on the samples. The rods have load cells built in, which allow to measure and log friction forces. The cam discs contain two halves each. The halves – discs are bolted together. By turning one of them with regard to the other one, the eccentric distance increases, which results in higher deflection amplitude. The deflection value is determined by pre-drilled holes in the discs and ranges from 0,5 mm to 12 mm. A Linear Variable Differential Transformer (LVDT) logs the deflection and number of bending cycles. By disconnecting a rod from the dolly, a specific load value can be set and fixed to ensure static bending conditions during test.

Friction wear is introduced to the system by means of Ø4.76 mm alumina ball fixed in a wear block located under the sample and with two rods fixed to it at the sides. The rods are covered with rubber lining to prevent current flow on the outside of the chamber, and are connected to a crankshaft, which in turn is connected to an electric AC motor by means of transmission chain and gear. Rubber bell sleeves are fixed to the cell and are touching the rods providing water-tight system. The wear block is pressed against the sample by a dead weight hanging on a line supported by pulleys and fixed to the wear block. Thanks to that at every point of test contact between the wear block and the sample in ensured. The reciprocating sliding amplitude is 20 mm. Both motors are controlled by a frequency converter, which allows adjusting cyclic deflection and sliding wear frequency. Another LVDT is used to log number of wear cycles.

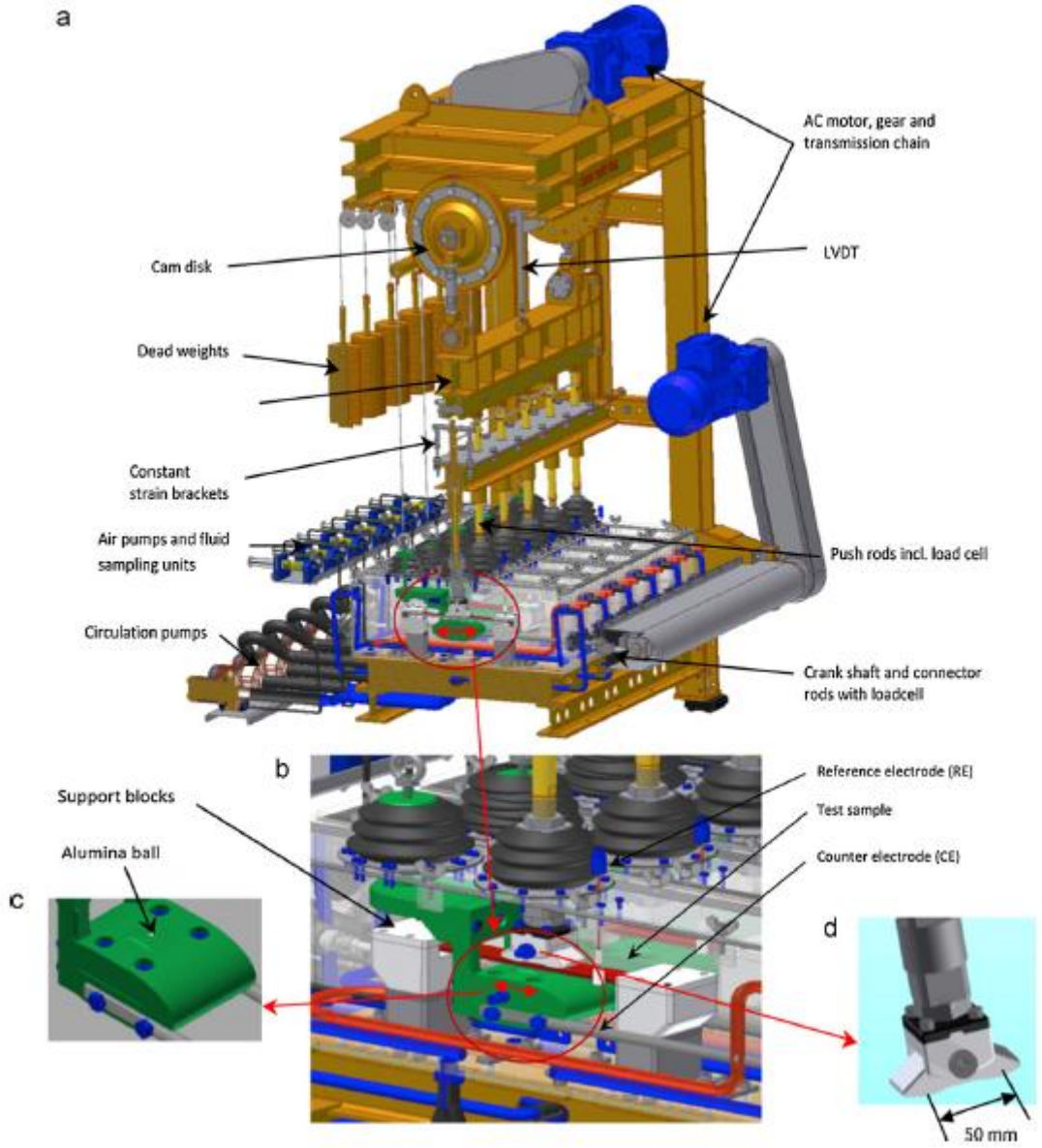

Fig. 3. (a) 3D model of the multi-degradation test rig. (b) Close up of test chamber (c) Wear block including alumina ball. (d) Free-floating dual load applicator including adjustment turnbuckle [48].

Test chamber

The test chambers constituting electrochemical cells are made of Lexan. It is transparent to allow visual monitoring of the system during the test. It is also chemically resistant. Test chamber can be covered to protect against splash, prevent electrolyte evaporation and contamination and also heat loss. Chamber dimensions are 720 mm x 135 mm x 230 mm. To fully immerse a sample in the electrolyte, 15 l of it is necessary. The chambers are equipped with nozzles connected to aerating pumps and circulation pumps. The former are responsible for simulating aerated splash zone conditions, the latter keep the electrolyte well stirred. This

ensures homogenous electrolyte composition and removal of generated debris from the ball/metal interface. Each chamber is connected to a separated air and water pump. The chambers are also equipped with heating system to control electrolyte temperature.

Test rig operation

The LSMD test rig is operated by use of a PLC system located in a cabinet at the side of the test rig. A computer is connected to the PLC control cabinet and logs all the input sensors: deflection, bending strain, friction loads, temperature, and bending and wear cycles. The system determines bending and wear frequency.

The multi-degradation tests are performed on flat samples with dimensions: 400 mm x 30 mm x 10 mm (fig. 4). Cylindrical test samples can also be used, maximum allowable size is 20 mm x 450 mm, indicating outer diameter and length, respectively.

Before carrying out a test, the sample needs to be polished to pre-defined roughness, an electrical wire has to be attached and an organic coating (paint) applied. A 15 cm^2 area at sample mid-length is left uncoated to be exposed to multi-degradation.

Tests are usually performed at applied load of 90% of material yield strength.

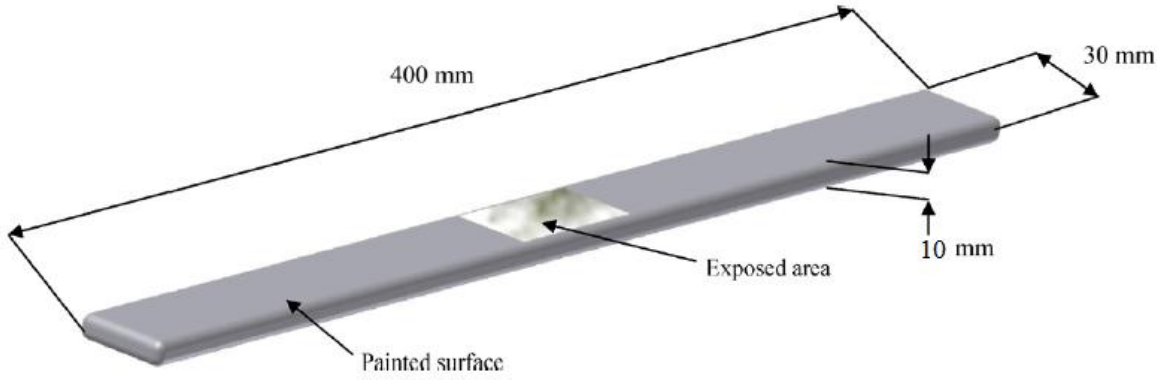

Fig. 4. Typical test sample size 400 mm × 30 mm × 10 mm, exposed area 15 cm^2 [48].

2. Experimental procedure

2.1. Material

Materials tested within this master thesis were AISI 316L austenitic stainless steel (UNS S31603) and 25% Cr super duplex stainless steel (UNS S32750), throughout this thesis referred to as ASS and SDSS, respectively. Chemical composition and properties of both materials are presented in tab. 1.

Metal alloy	Chemical composition [wt%]	$R_{p0,2}$ [MPa]	PRE_n
ASS (UNS S31603)	0.019 C, 1.36 Mn, 0.034 P, 0.002 S, 0.32 Si, 16.8 Cr, 10.04 Ni, 2.0 Mo, 0.036 N [49]	262	24
SDSS (UNS S32750)	0.015 C, 0.85 Mn, 0.022 P, 0.001 S, 0.28 Si, 25.0 Cr, 6.88 Ni, 3.8 Mo, 0.29 N, 0.2 Cu [50]	563	42.2

Tab.1. Chemical composition and properties of the test sample materials.

PREn was calculated based on eq. (10). Test samples size was 400 mm x 30 mm x 10 mm. Samples were polished with sand paper with stepwise decreasing grain size and finished at grit size P1000. Samples were washed in acetone, ethanol and distilled water ultrasonic bath, in order to get rid of all contaminants and provide adherence of the coating. The coating used was epoxy paint Jotamastic 90, Jotun [51]. Heat-shrinkable tubes was used on both ends of samples to prevent coating delamination under cyclic bending and thus potential reading disturbance.

2.2. LSMD test rig

Sample was fixed in the supports, then bending load was applied and the normal load pressing the alumina ball to the sample as well. The wire attached to the sample was as the sample works as the working electrode in this system. A reference electrode was place in the electrolyte to measure the cell potential. For both materials tests the following parameters were adjusted:

- ✓ Normal load: 30 N, 50 N, 70 N

- ✓ Bending conditions: no bending (tribocorrosion), 90% $R_{p0,2}$ static bending, 90% $R_{p0,2}$ cyclic bending with frequency 1,25 Hz

For each normal load-bending condition combination one test was performed, resulting in combined amount of 18 tests. All tests were performed for a period of time of 7200s and sliding frequency of 1Hz, meaning 7200 wear cycles.

For all tests 3.4 wt% NaCl solution was used as electrolyte. The weight percentage of NaCl is assumed to simulate conditions prevailing in the North Sea (34‰ salinity).

2.3. Volume loss measurements

After test samples were cleaned with distilled water, then the middle part of the sample was cut off by means of manual cutting machine. Obtained sample was cleaned in ethanol and distilled water ultrasonic bath and dried. Volume loss measurement and wear track profile reading was performed by means of confocal microscopy (IFM ,Alicona). The wear track was scanned and the reference plane was set at the level of not corroded material outside the wear track. The volume loss was measured by measuring mean depth and width and then assuming a triangle as the cross-section of the wear track. The wear track transversal profile was measured at mid-length. Vertical resolution was set at 410 nm, 10x magnification was used.

2.4. Electrochemical measurements

During tests the OCP was measured. Ag/AgCl reference electrode was used. The potential was measured 10-15 min before test star-up to stabilize, also after the test the potential was measured for 5 min to observe the repassivation response.

2.5. Hardness measurements

The microhardness $HV_{0.1}$ was measured for all samples both inside and outside wear track. The indentation load was 100gf with duration time of 15s. The equipment used was Mitutoyo HM-200 series micro Vikers hardness testing machine.

2.6. Surface, subsurface and morphology characterization

2.6.1. FIB/SEM

The morphology and subsurface microstructure or the wear track (in the mid-stroke location) was studied using FIB (by using FEI Helios NanoLab DualBeam FIB) and SEM (by using cross beam microscopy). Gallium liquid metal ion source was used for milling, polish and deposition in order to perform and analyze longitudinal and transversal cross-sections. The electron beam conditions were set at: accelerating voltage 10 kV and beam current 0.17nA.

2.6.2. XPS

Surface composition was analyzed by means of XPS by using Kratos Axis Ultra DLD and monochromatic Al Kα source (15 mA, 15 kV) was used for spectrometry. The reference sample for depth measurements was Ta/Ta_2O_5. Casa XPS software was used for analyzing and curve fitting of XPS data and Shirley background subtraction [58] was used for all the evaluations and quantifications of the data.

3. Results

3.1. Chemical and electrochemical behavior

3.1.1. OCP evolution

ASS

Fig. 5 and fig. 6 show the OCP evolution on ASS at tribocorrosion (reference) and multi-degradation conditions, and the potential drop representation for each load-strain state combination, respectively.

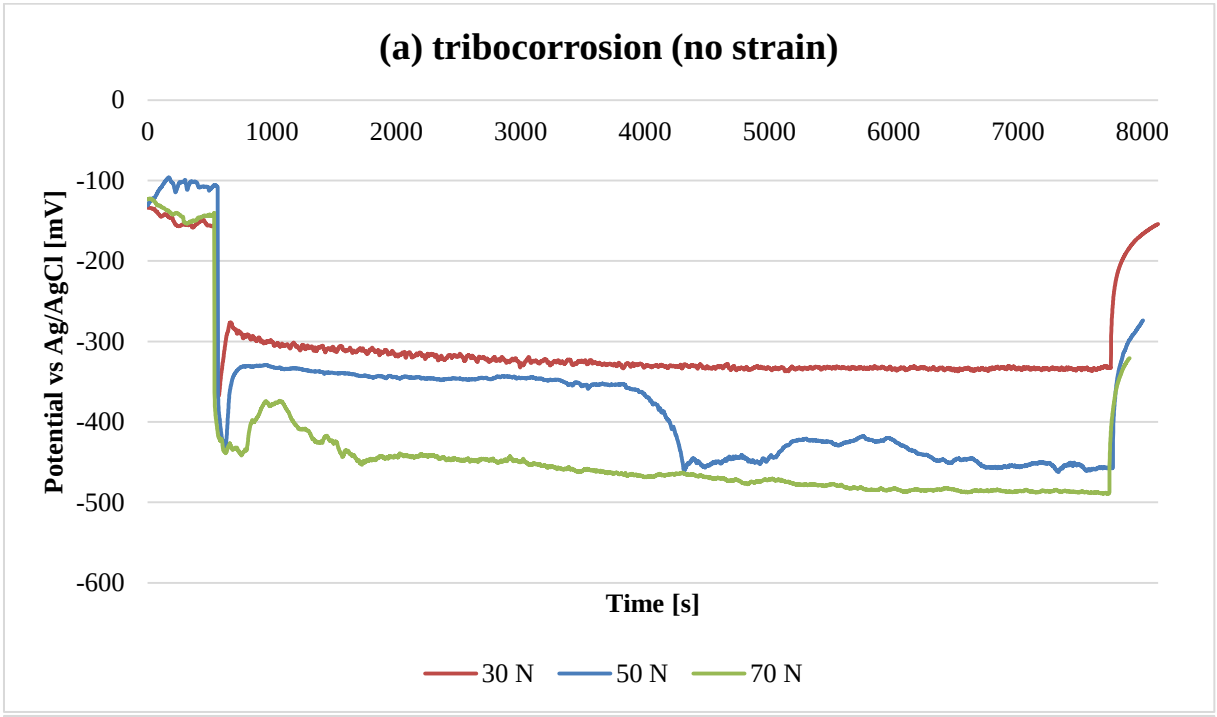

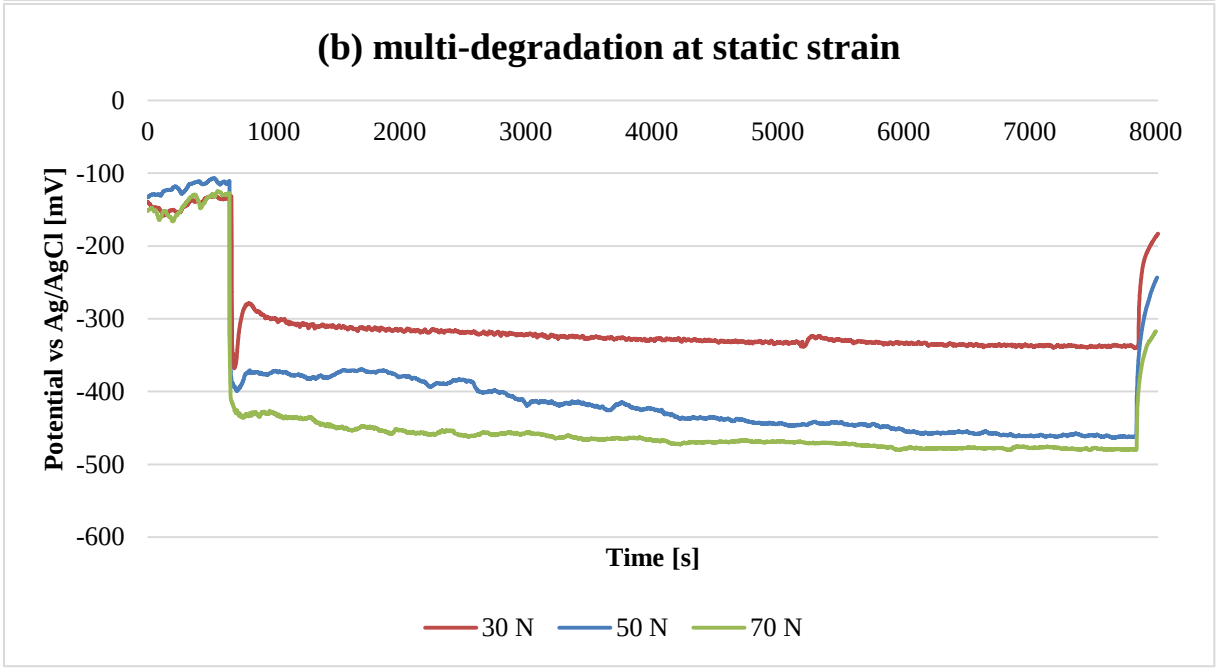

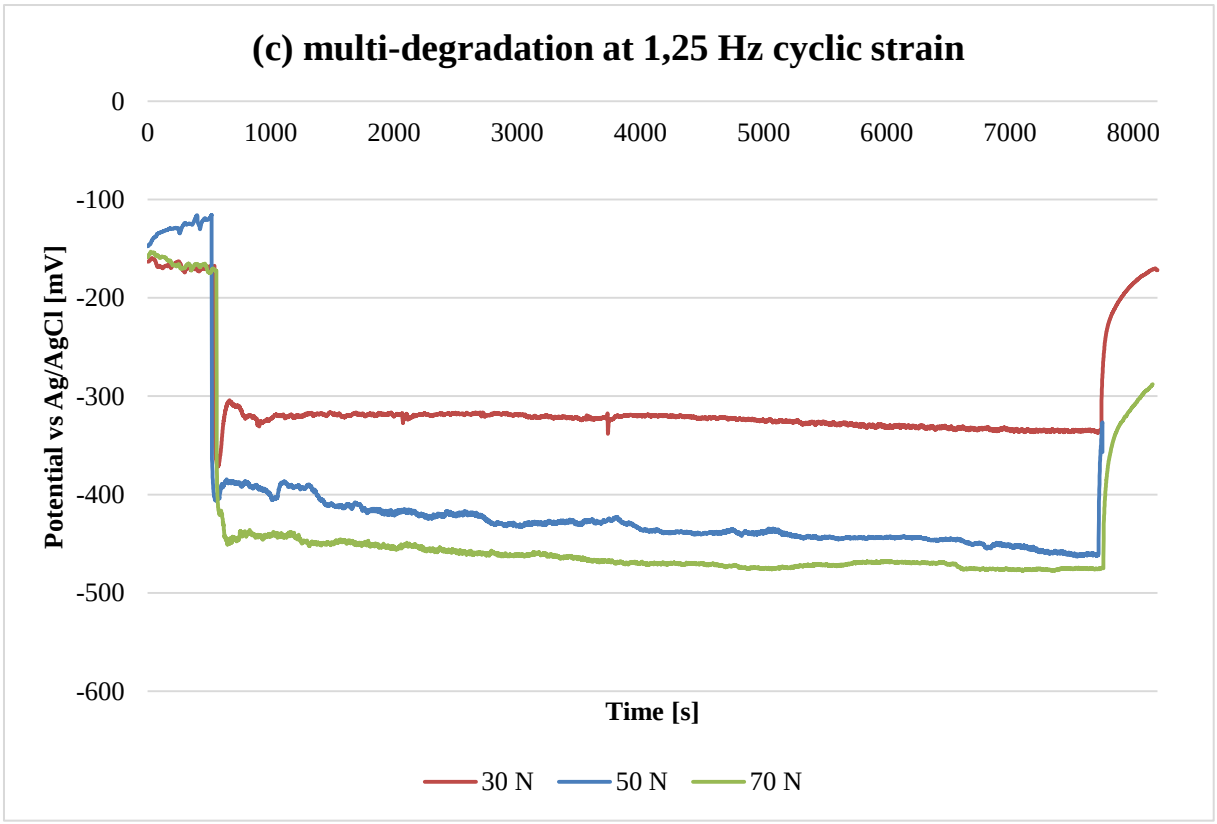

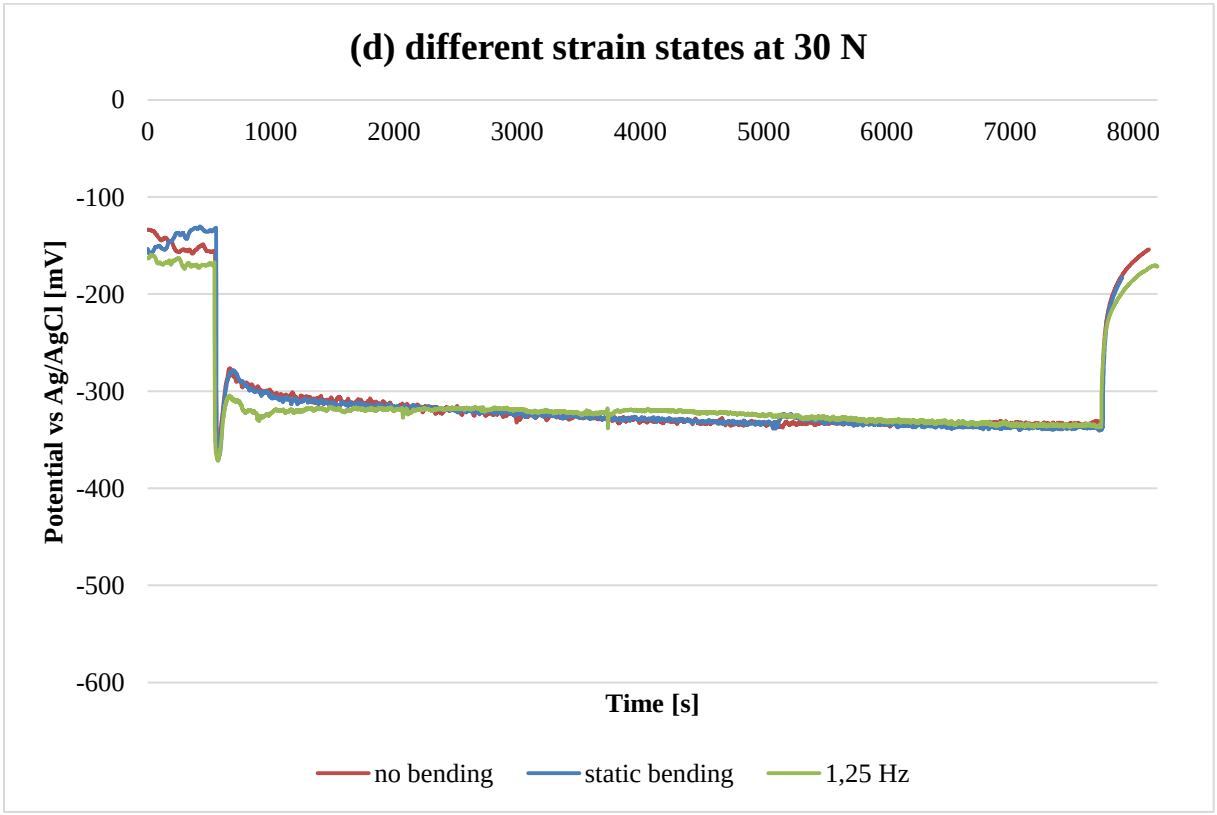

Fig. 5. OCP evolution of ASS during (a) tribocorrosion and multi-degradation at applied: (b) static strain (c) cyclic strain with frequency 1,25 Hz and (d) at different strain states at fixed normal load of 30 N.

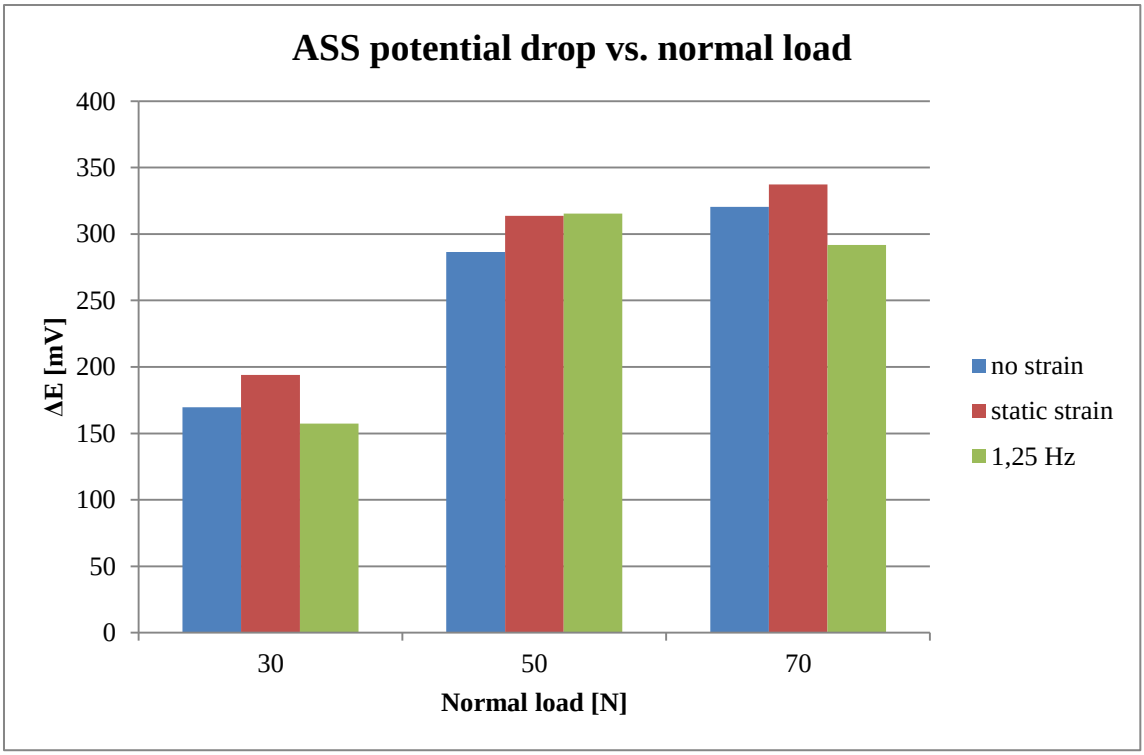

Fig. 6. Potential drop measured on ASS during tribocorrosion/multi-degradation tests at different normal loads and strain states.

Fig. 5a-c show the influence of applied normal load on OCP – by increasing the normal load, the OCP decreases. This trend was observed for tribocorrosion as well as for multi-degradation, both at applied static strain and cyclic strain. Fig. 6 in turn gives an estimation of potential drop at the onset of rubbing or rubbing combined with applied strain, which refers to tribocorrosion or multi-degradation, respectively. A trend can be observed – the higher the load, the higher the potential drop, which implies higher anodic dissolution rate. This is explained by higher contact stresses and more intensive wear and thus deeper ploughing of the ball and exposing bigger metal area to dissolution. Also, for each normal load value the potential drop value at static strain exceeds the one for no strain (tribocorrosion). Such behavior was expected, since at applied static strain (possible) cracks may appear (and be open), which increases the area exposed to dissolution and thus its rate.

Also, the same OCP value during test is noted at different strain states at fixed normal load value, as depicted at fig. 5d. Only the reading at 30 N is attached, however the trend occurs at all normal load values.

SDSS

Fig. 7 and fig. 8 show the OCP evolution on SDSS at tribocorrosion (reference) and multi-degradation conditions, and the potential drop representation for each load-strain state combination, respectively.

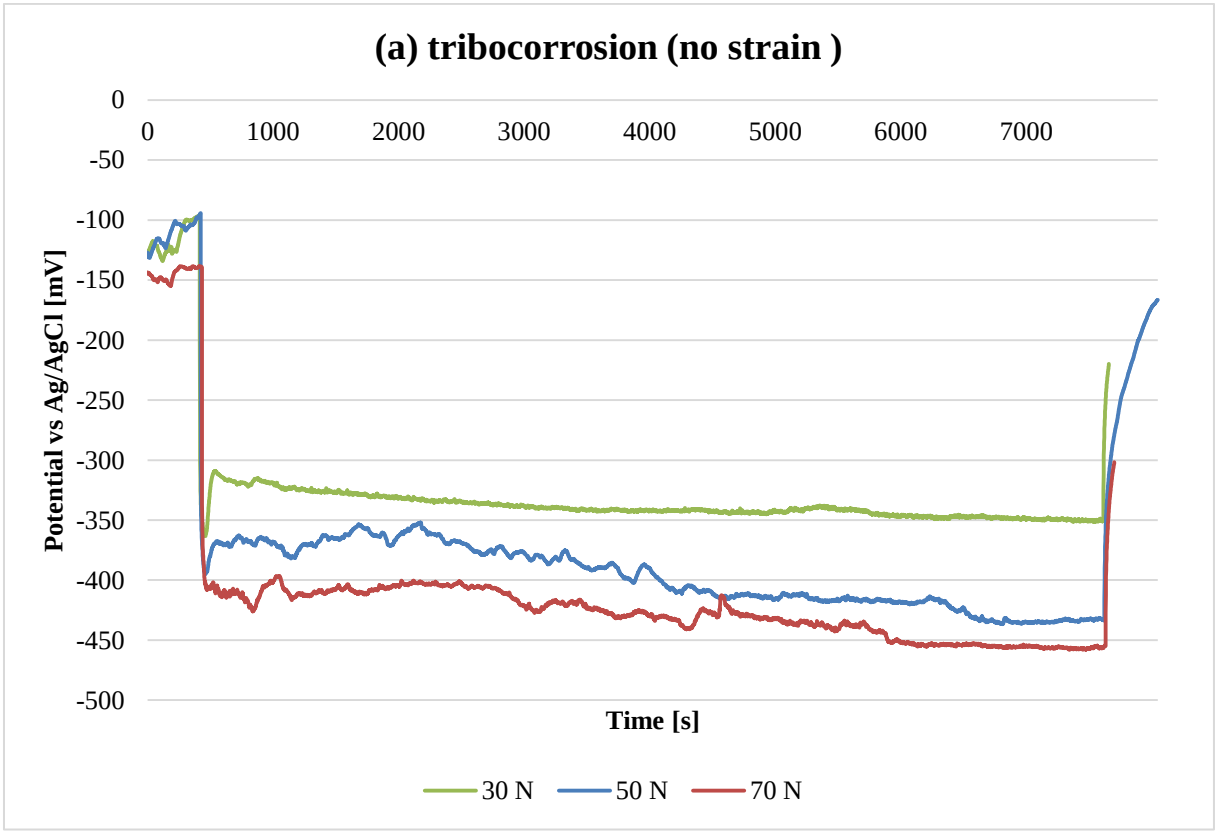

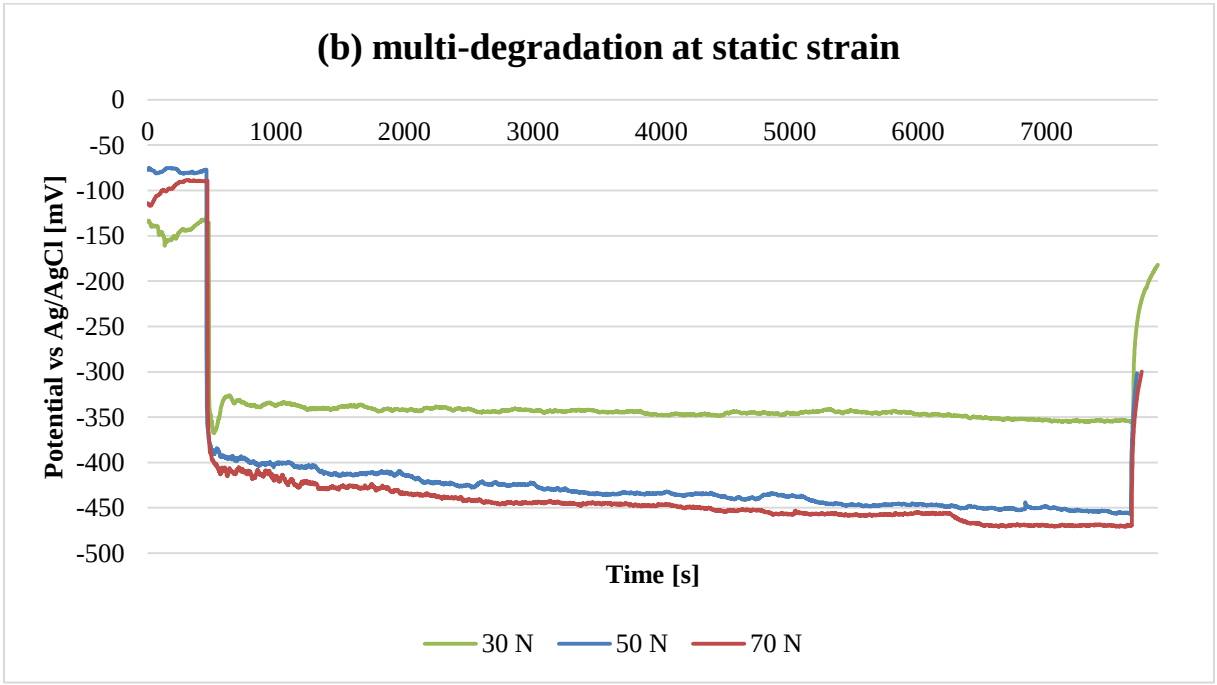

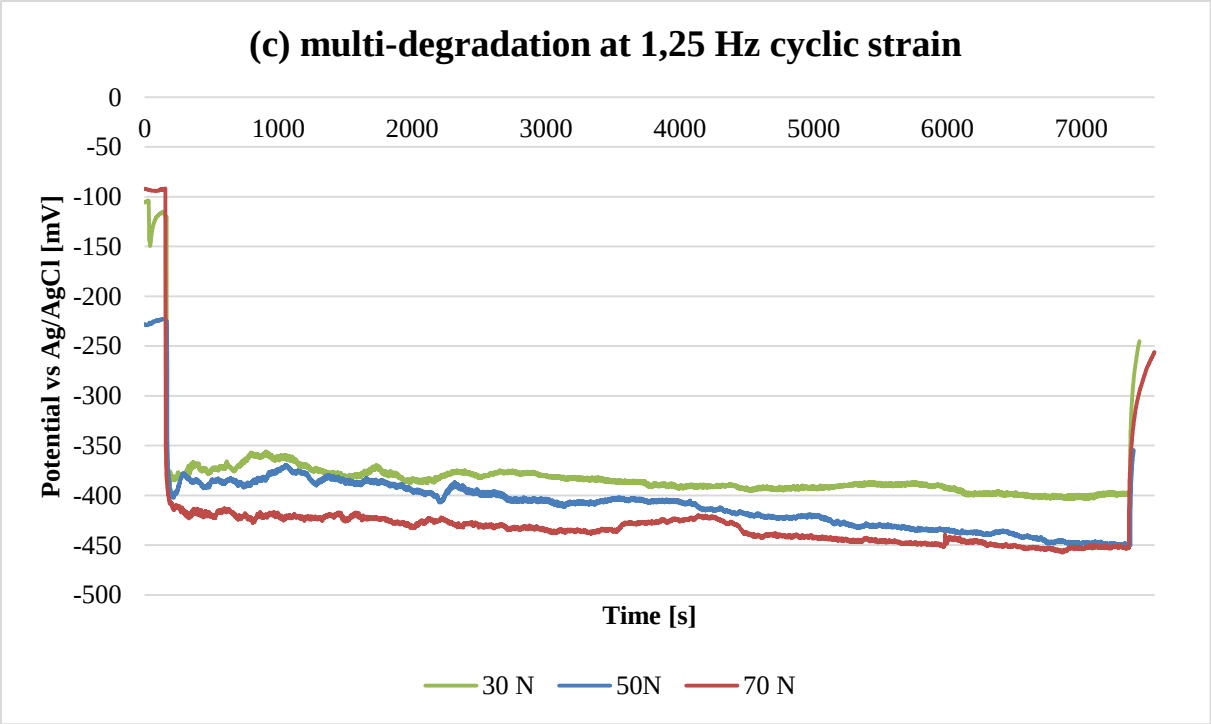

Fig. 7. OCP evolution of SDSS during (a) tribocorrosion and multi-degradation at applied: (b) static strain and (c) cyclic strain with frequency 1,25 Hz.

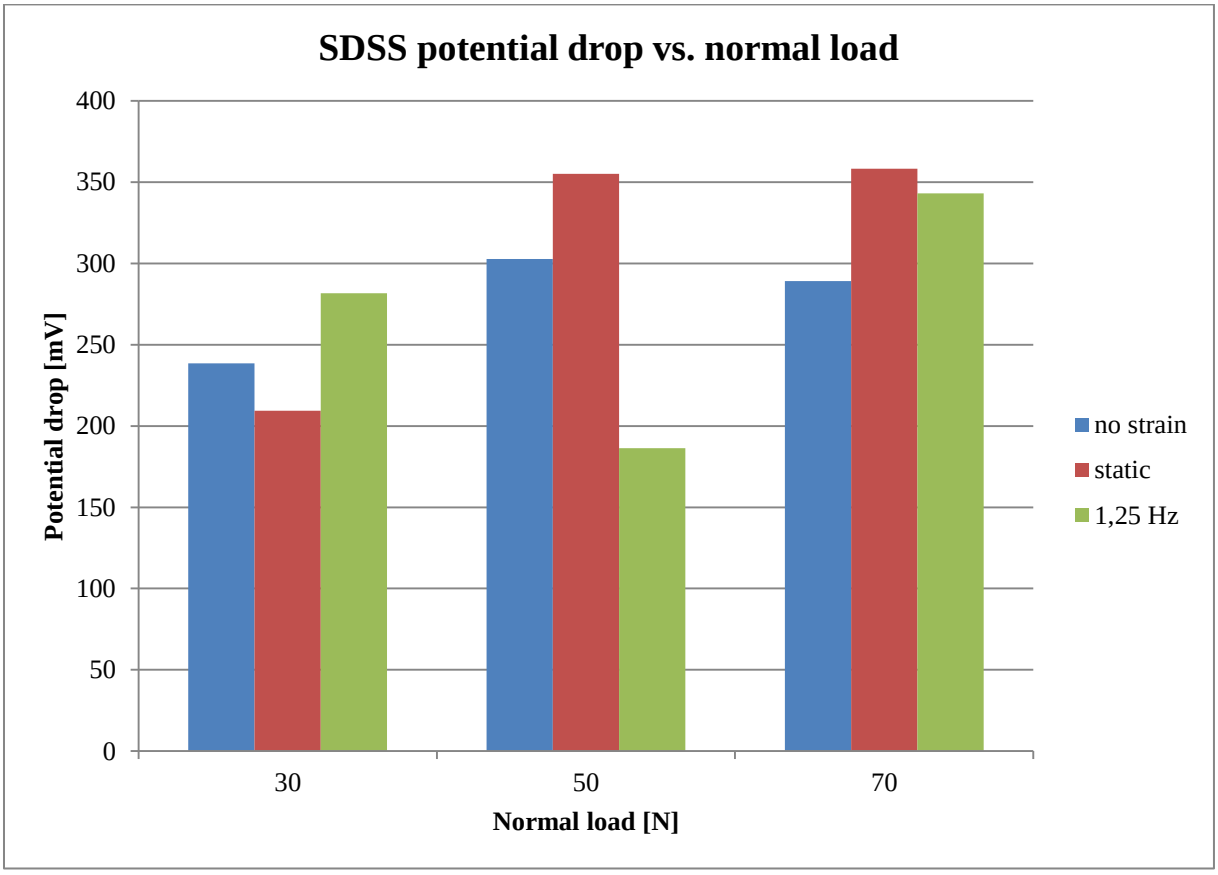

Fig. 8. Potential drop measured on SDSS during tribocorrosion/multi-degradation tests at different normal loads and strain states.

The same trend as on ASS can be observed: the higher normal load, the lower the OCP during tribocorrosion or multi-degradation exposure (fig. 7). Also, the potential drop value increases at applied static strain compared to tribocorrosion (at 50 N and 70 N normal load, fig. 8). It is attributed to the same mechanisms as on ASS.

OCP exhibits different behavior on SDSS than on ASS – its value does not settle at the same level at different strain conditions. One tendency can be spotted – OCP at applied strain (both static and cyclic) is lower than at no strain state (tribocorrosion), which is observed for all normal load values. However, values at static and cyclic strain vary and there is no obvious correlation between them.

3.1.2. Surface composition

In tab. 2 passive film thickness at different strain states is presented, both on ASS and on SDSS.

	no strain	static strain	cyclic strain (1,25 Hz)
ASS	6,1	7,6	6,14
SDSS	3,6	4,6	2,8

Tab. 2. Passive film thickness [nm] on ASS and SDSS at different strain states at 50 N normal load.

ASS

Passive film formed at ASS surface is thickest at applied static strain – 7,6 nm, and exhibits very similar values at tribocorrosion - 6,1nm - and cyclic strain state – 6,14 nm (tab.2).

Fig. 9 shows the atomic concentration of iron and chromium cations in the passive film present at the surface of ASS outside and inside the wear track. Distinct trend in chemical segregation at the surface was observed at tribocorrosion exposure within the wear track (fig. 9b) compared to the surface outside (fig. 9a) - the content of chromium oxides and hydroxide increases, whereas the content of iron oxides decreases. At applied static strain the variance is higher and at cyclic strain it increases even more. Chromium oxide present on the surface is hard, however the indenter during microhardness measurement goes deeper into the material than the passive film depth (couple of nm), so it does not affect the microhardness.

The chemical (cation) composition does not vary significantly with distance from the surface – the content of chromium-containing compounds remains high and containing iron low, which occurs at every strain state.

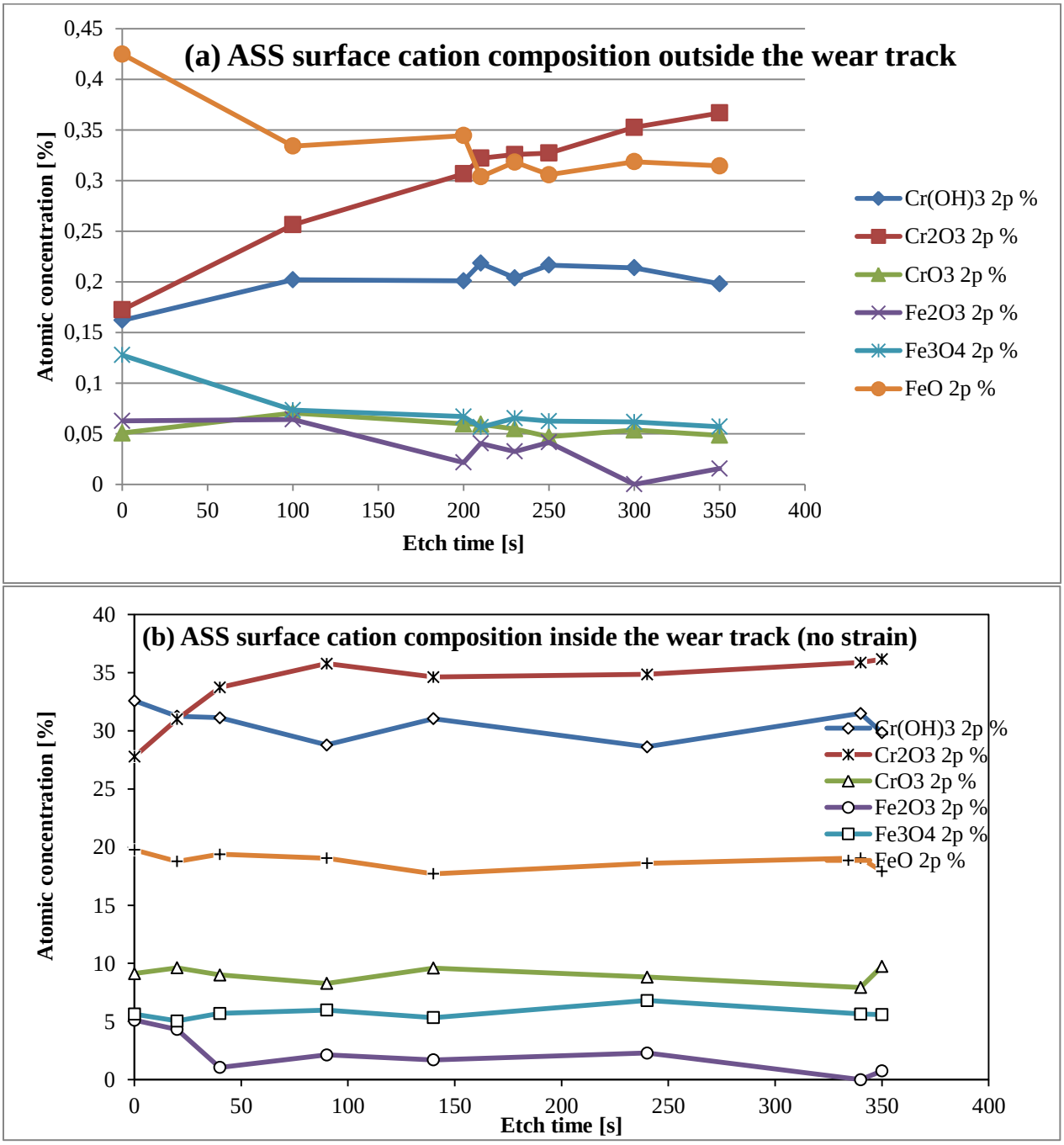

Fig. 9. Surface cation composition of ASS: (a) outside the wear track at 50 N normal load and (b) inside the wear track at triborossorion exposure (no strain).

Fig. 10 depicts chemical composition at the wear track surface. One can see high oxide content on the surface (72-75% depending on strain state), which represents oxide surface layer. With the distance from the surface oxide content drops, whereas chromium and iron content increases (from 13-17% and 6-10% on the surface, respectively). Molybdenum and nitrogen content is very small (0,4-1,4% and 0,3-0,9%, respectively) and does not significantly vary with the distance from the surface. However, even small molybdenum content was reported to have influence on stainless steel corrosion resistance [52,53,54]:

- ✓ Higher Mo content increases pitting corrosion resistance – PRE_n (eq. (10) in section 1.2.2.3),
- ✓ Higher Mo content results in thicker more stable passive film (of higher integrity).

Obtained values back this theory up – PRE_n calculated from eq. (10) at no strain, static strain and cyclic strain equals 25.3, 34.6 and 26.8, respectively. Trend in these values corresponds with passive film thickness in tab.2. This proves that XPS measurements were carried out propery.

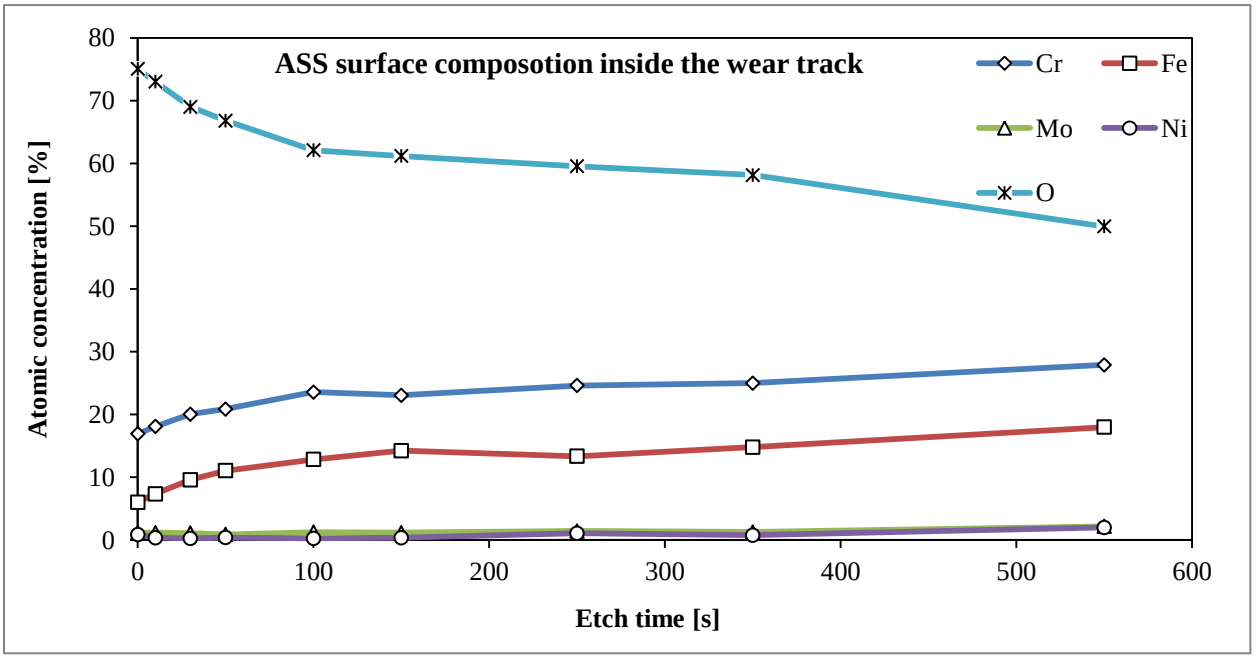

Fig. 10. Surface chemical composition of ASS inside the wear track at static strain and 50 N normal load.

SDSS

The passive film exhibits similar trend as on ASS (tab. 2) – it is thickest at applied static strain – 4.6 nm, and thinner for no strain and cyclic strain – 3.6 nm and 2.8 nm, respectively. Obtained values are lower than corresponding ones on ASS.

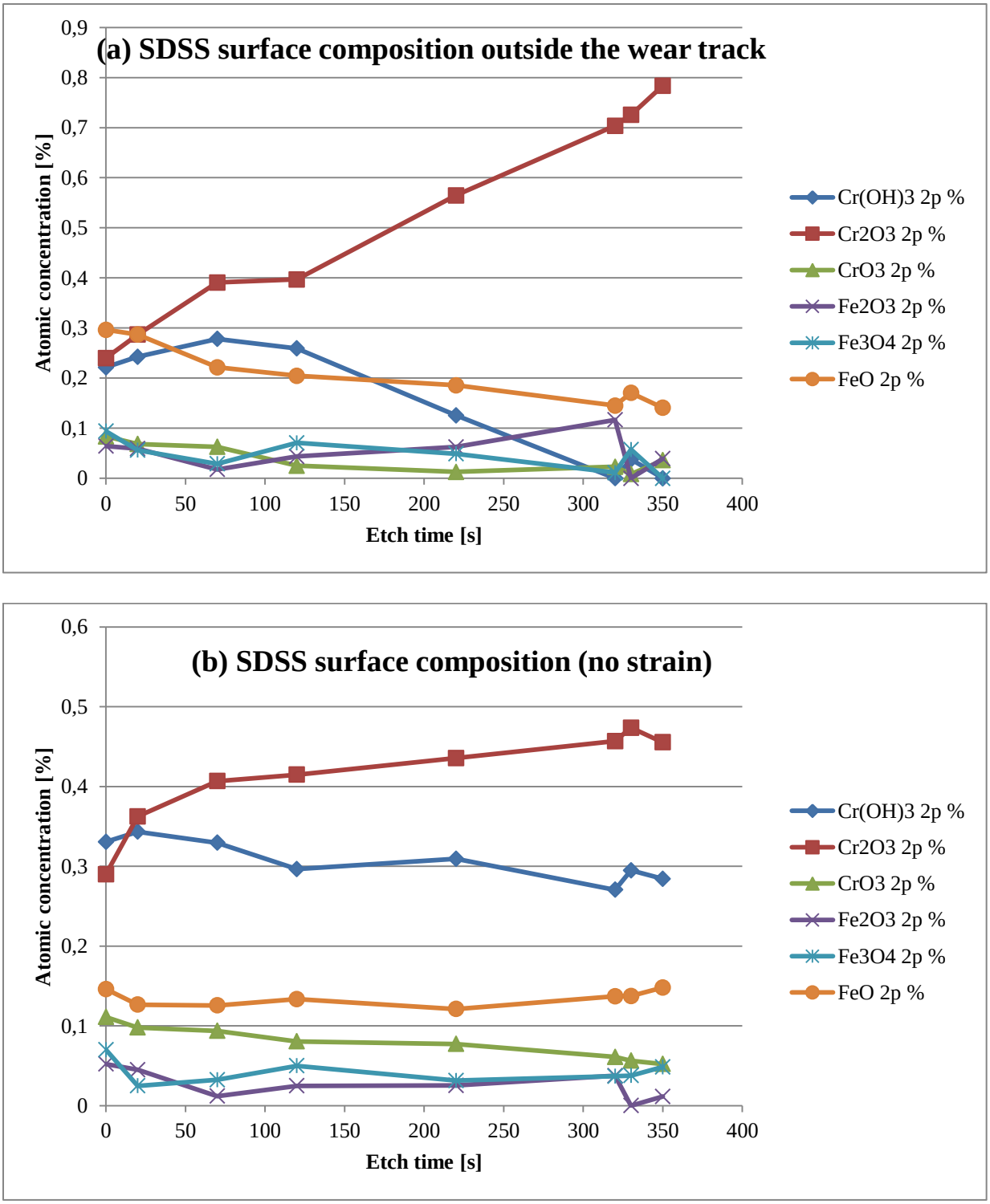

Fig. 11. Surface cation composition of SDSS: (a) outside the wear track at 50 N normal load and (b) inside the wear track at triborossorion exposure (no strain).

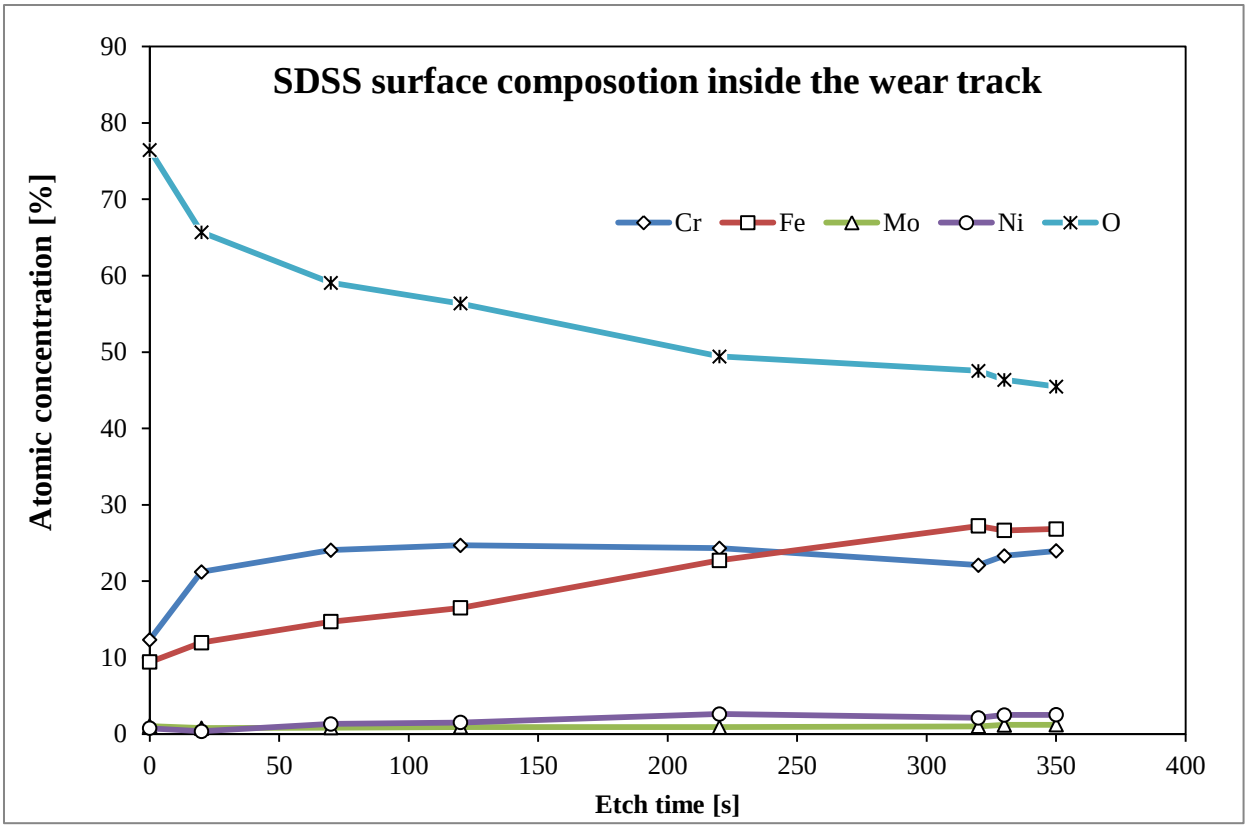

Fig. 12. Surface chemical composition of ASS inside the wear track at static strain and 50 N normal load.

Outside the wear track the surface composition in dominated by chromium compounds (fig. 11a). At tribocorrosion exposure the content of chromium-containing compounds increases, while iron-containing decreases (fig. 11b). These values remain relatively stable for other strain states, with only slight variations. Like on ASS the chromium-containing/iron-containing compound ratio is quite stable across the material depth at all strain states. A hard oxide layer is formed on the surface, harder inside (due to higher Cr content) than outside the wear track, however, like on ASS, it does not influence measured microhardness.

Chemical composition influences the corrosion resistance of SDSS, which is directly related to passive film thickness. Molybdenum was reported to have pronounced influence on passive film formed on duplex stainless steels [54]. Duplex/super duplex stainless steels consist of two phases: molybdenum-rich ferrite and nitrogen-rich austenite, and the interaction of these elements contributes to the corrosion resistance. PREn calculated as for ASS amounts to: at no strain (tribocorrosion) 18.8, at static strain 27.6 and at cyclic strain 9.62. Again, as on ASS, the trend in these values corresponds with passive film thickness in tab. 2.

3.2. Multi-degradation behavior

3.2.1. Volume loss and wear track depth

ASS

Fig. 13 depicts volume loss obtained as a result of tribocorrosion and multi-degradation tests carried out on ASS. At all strain states a similar trend appears, meaning the higher the normal load, the bigger the volume loss. This is attributed, as well as the higher potential drop, to deeper alumina ball ploughing into the steel resulting from higher contact stresses. Also, at 50 N normal load another tendency was observed – the volume loss increases as the static strain is applied, and it increases even more at applied cyclic strain with frequency 1,25 Hz. However, at 70 N exactly reversed trend was observed, meaning the highest volume loss at tribocorrosion conditions and its decrease at applied static and cyclic strain, respectively. At 30 N it is hard to assume some trend, since the values are nearly negligible and differences between them are small, which makes them not very reliable.

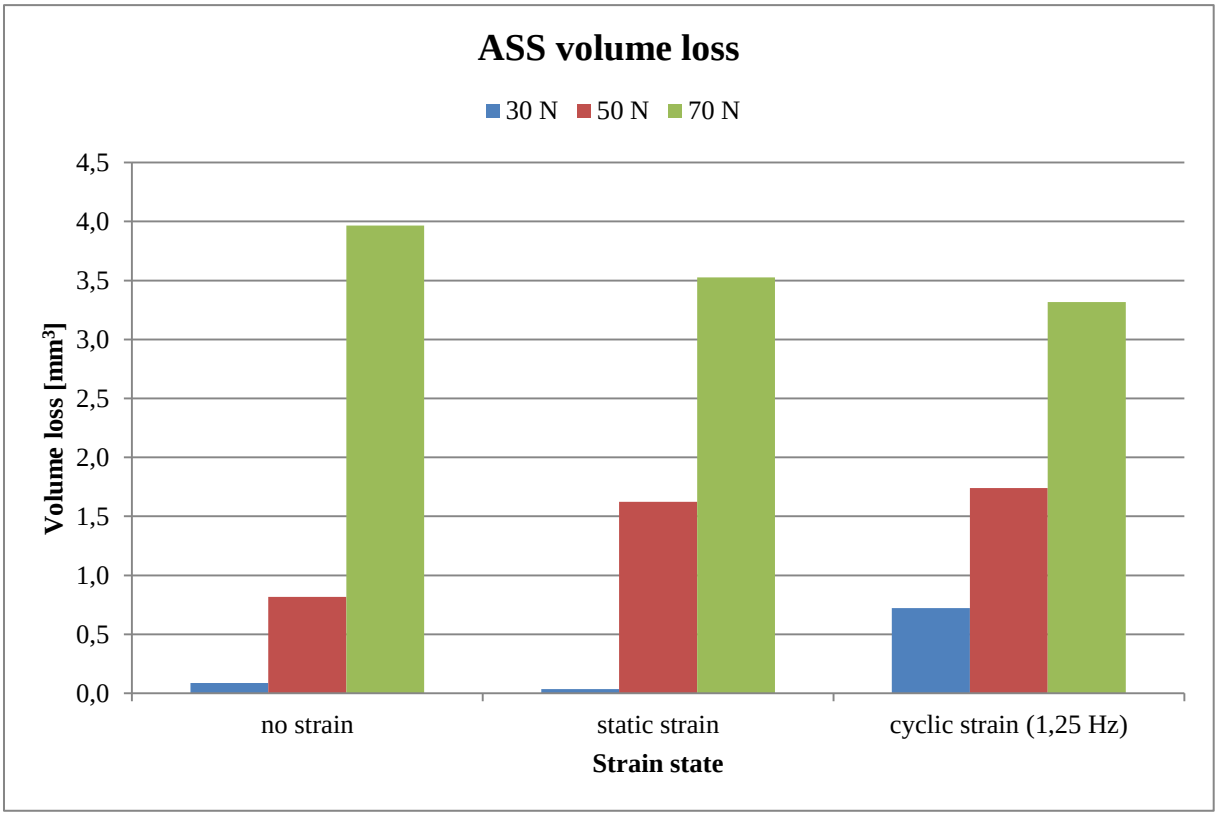

Fig. 13. Volume loss measured on ASS during tribocorrosion/multi-degradation tests at different normal loads and strain states.

Wear track transversal profile of each sample corresponds to volume loss depicted at fig. 13. The same trend occurs – the higher the normal load, the deeper the wear track.

SDSS

Fig. 14 presents SDSS volume loss data, which seems more consistent than on ASS. The same trend concerning normal load influence was observed – the higher load, the larger volume loss. Also, both at 50 N and at 70 N normal load the volume loss increases at applied static strain compared to no strain state (tribocorrosion – the reference) and then decreases at applied cyclic strain (here with frequency 1,25 Hz). This is the mechanism expected to occur [47]. As well as in case of ASS, at 30 N normal load the obtained values are nearly negligible and do not vary significantly.

Wear track transversal profile of each sample corresponds to volume loss depicted at fig. 14. The same trend as on ASS occurs – the higher the normal load, the deeper the wear track.

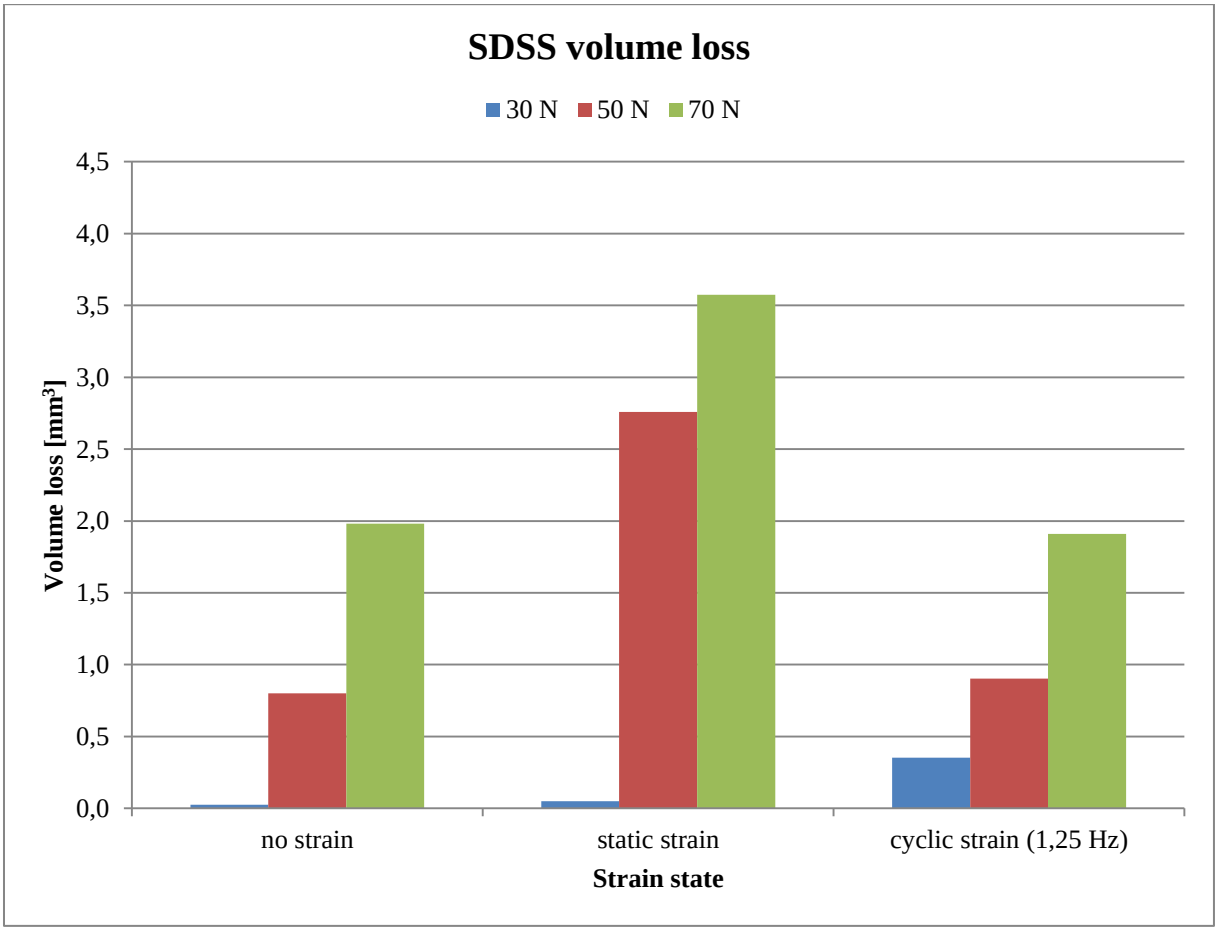

Fig. 14. Volume loss measured on SDSS during tribocorrosion/multi-degradation tests at different normal loads and strain states.

3.2.1. Microhardness response

ASS

There is no particular trend in terms of normal load or strain state influence on ASS surface microhardness except for the fact, that surface hardening occurs. It happens for all test conditions, inside the wear track, as depicted at fig. 15a. Outside the wear track the microhardness slightly varies from the reference value indicating either surface hardening or softening (fig. 15b). Also, microhardness tends to be higher inside the wear track rather than outside.

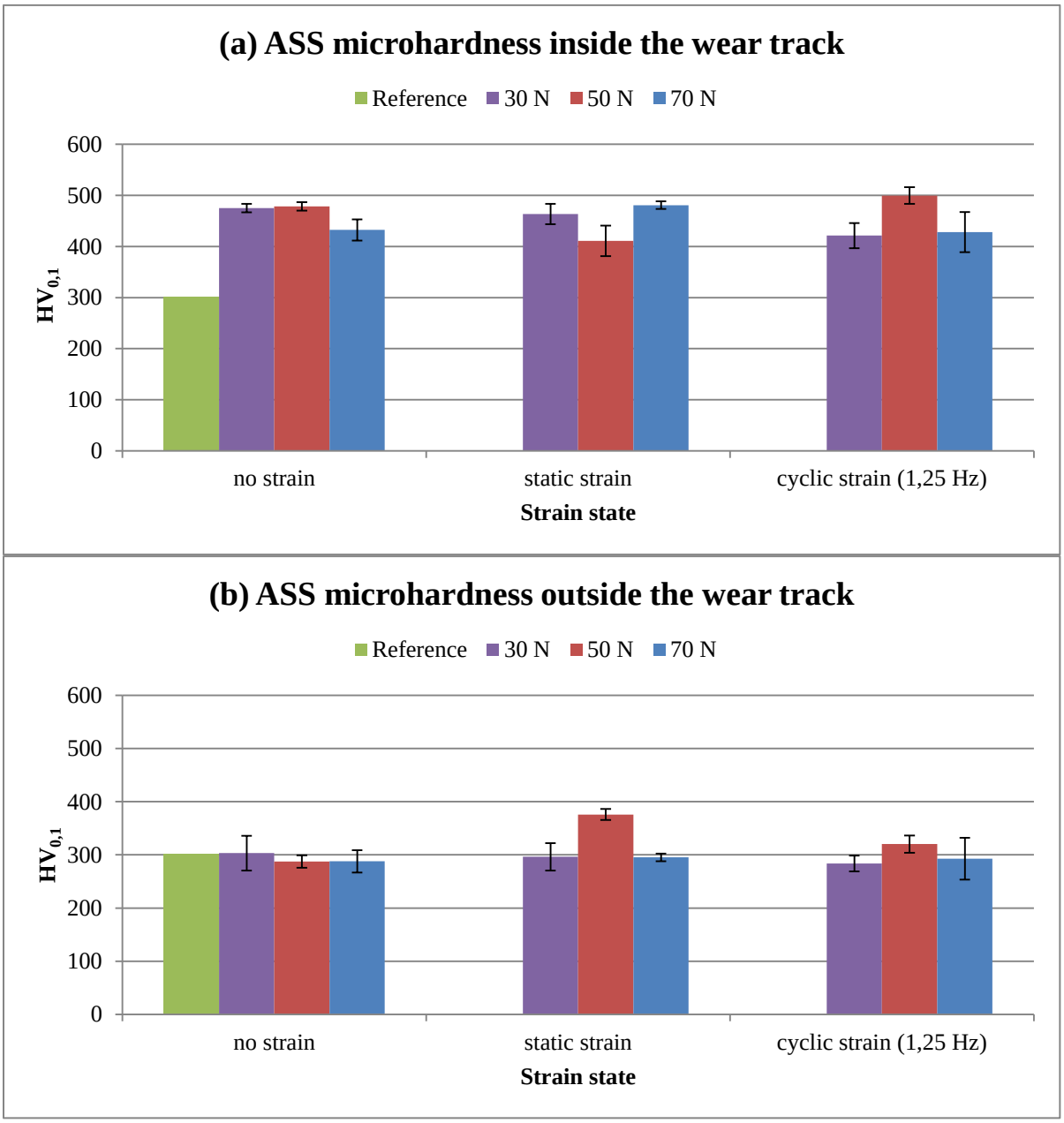

Fig. 15. Microhardness response after tribocorrosion and multi-degradation tests on ASS: (a) inside and (b) outside the wear track.

SDSS

Fig. 16 shows the microhardness response of SDSS on tribocorrosion/multi-degradation testing. As in case of ASS the surface inside the wear track work hardens during such kind of exposure, such behavior was observed on each sample. However, unlike ASS, the SDSS surface outside the wear track work hardens, though to lesser extent than in the inside. Finally, no trend linking the applied normal load or the strain state with microhardness response can be made.

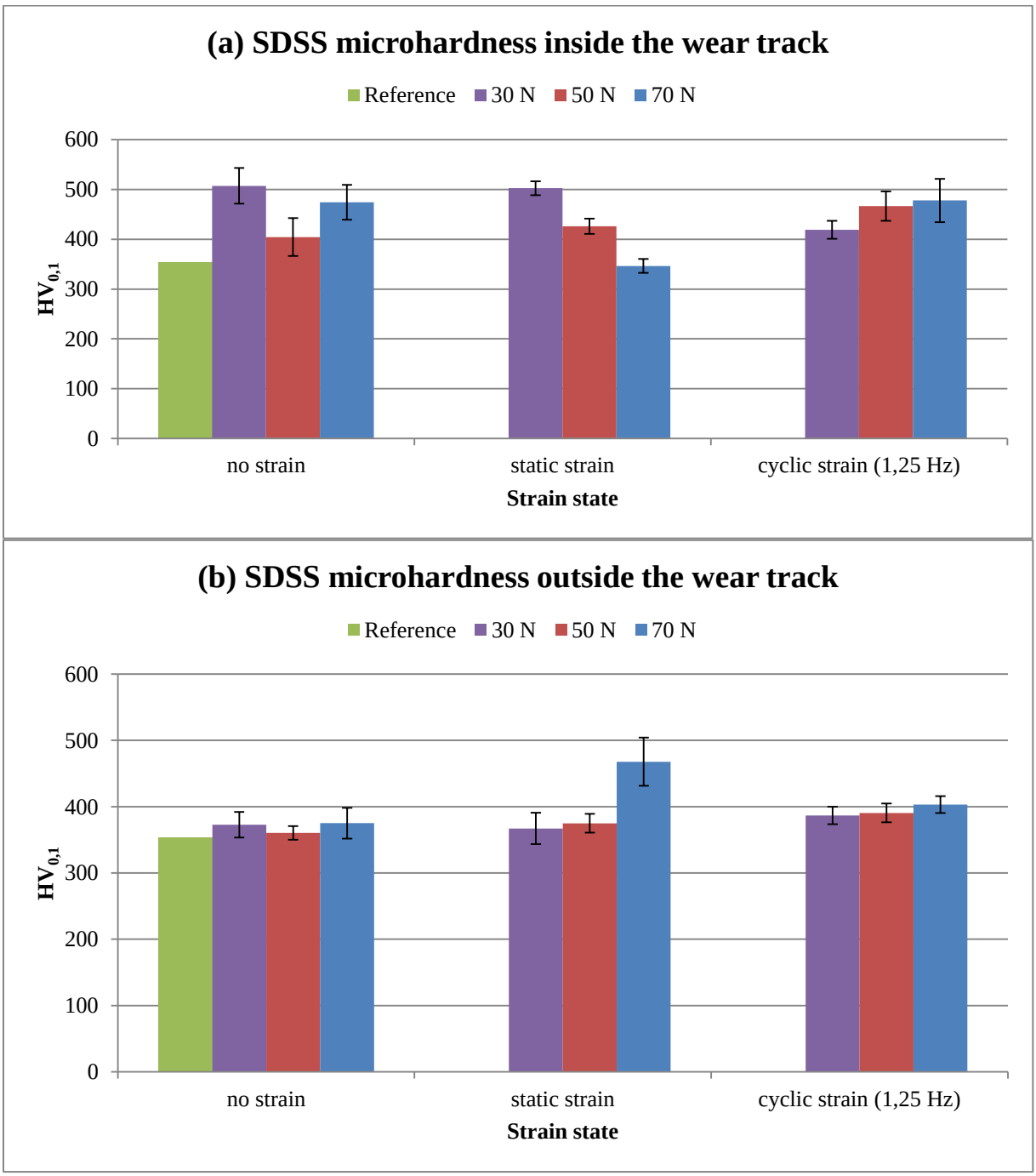

Fig. 16. Microhardness response after tribocorrosion and multi-degradation tests on SDSS: (a) inside and (b) outside the wear track.

3.2.2. FIB/SEM results

ASS

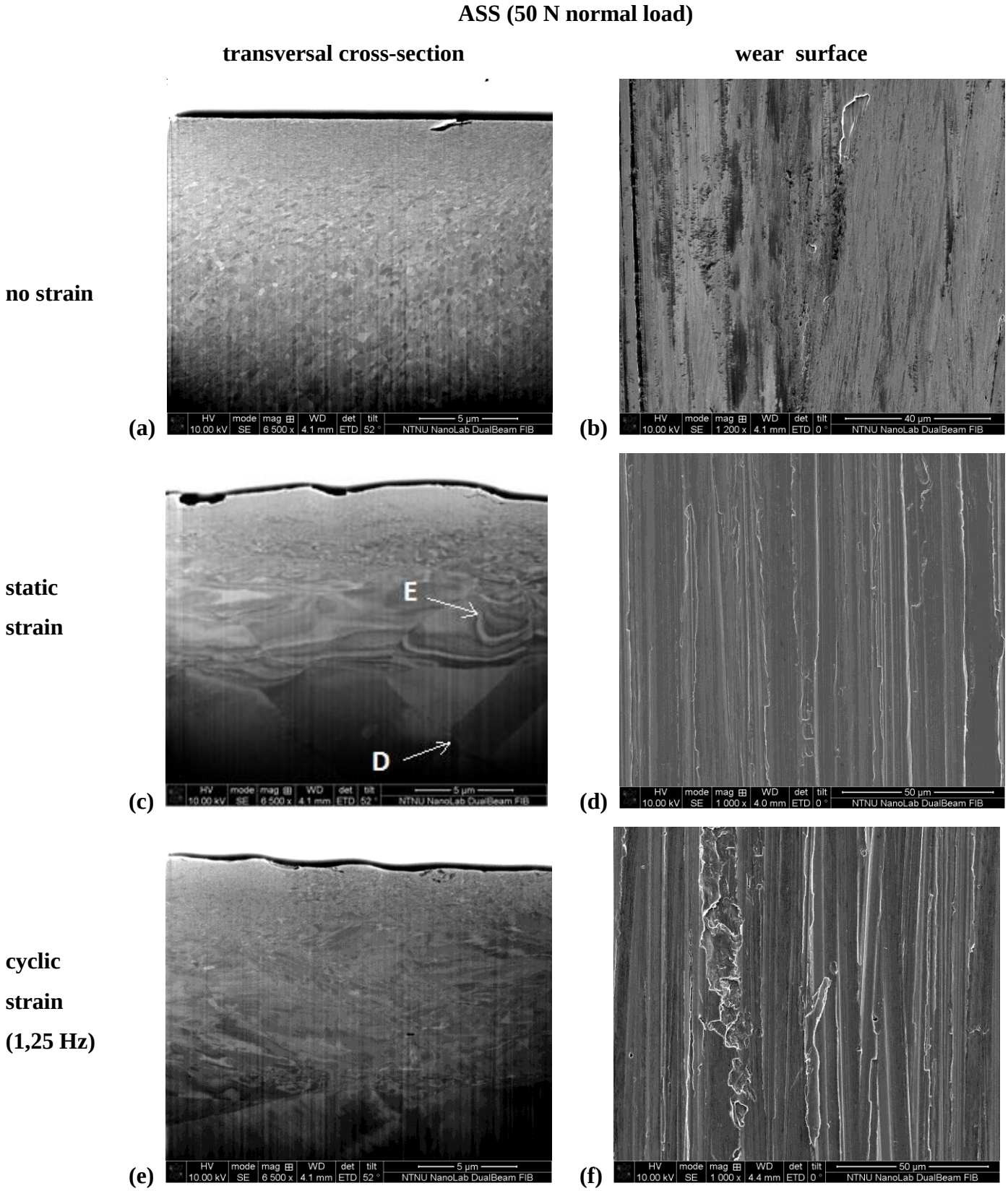

Fig. 17. SEM images of ASS wear tracks at 50 N normal load - surface images and transversal cross-sections.

ASS (70 N normal load)

transversal cross-section **wear surface**

no strain

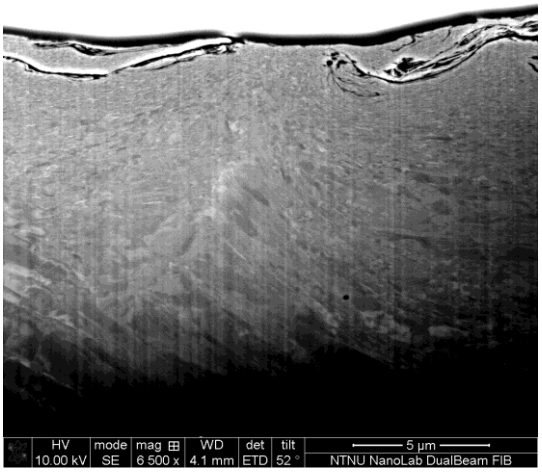

(a)

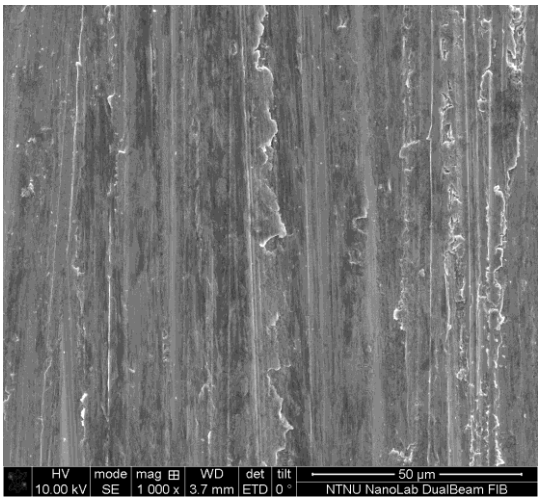

(b)

static strain

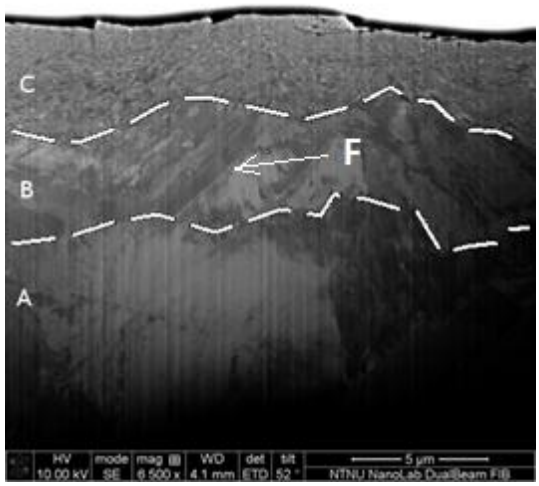

(c)

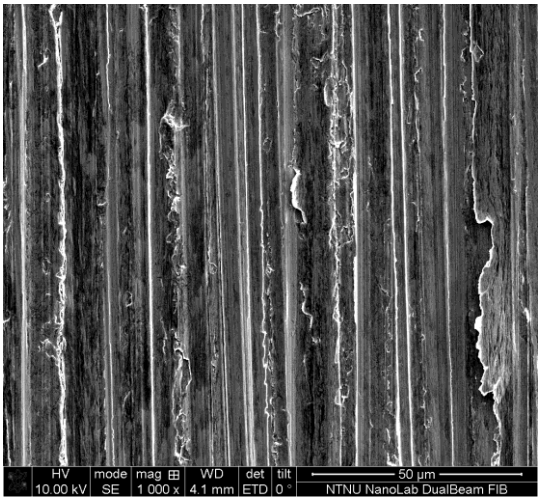

(d)

cyclic strain (1,25 Hz)

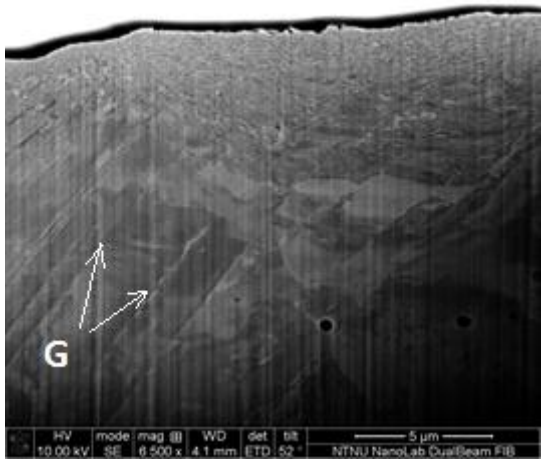

(e)

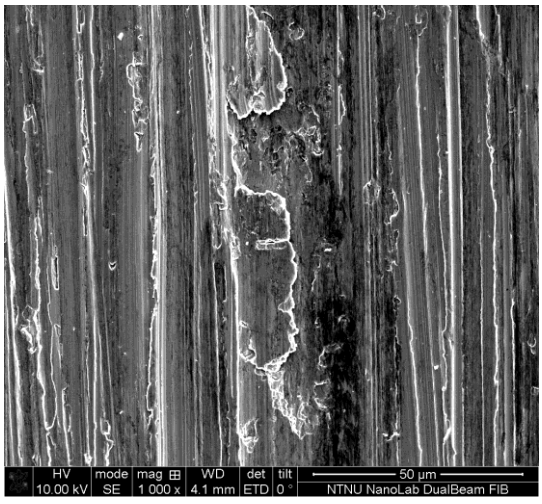

(f)

Fig. 18. SEM images of ASS wear tracks at 70 N normal load - surface images and transversal cross-sections.

The samples morphology is strongly affected by prevailing conditions, which is depicted at fig. 17 and fig. 18 referring to normal load of 50 N and 70 N, respectively.

All three zones mentioned in section 1.2.2.3 are possible to distinguish: the bulk material, the grain size gradient zone and the nanocrystalline subsurface layer (fig. 18c: A, B and C, respectively). Distinct boundaries between these zones are observed. As expected, the subsurface refined layer is much thicker at tribocorrosion conditions than at applied static strain (fig. 18a and 18c), which is attributed to higher stress dissipation after applying bending [40].

At tribocorrosion conditions (fig. 18a) large cracks can be observed, both surface and subsurface. Crack propagation occurred parallel to the surface, as it should in sliding contact; cracks are believed to origin from material chips being plastically deformed from the surface and then smeared back into surface during sliding. Without applied external strain cracks can propagate to larger extent, such behavior is not observed at static/cyclic strain state. At fig. 17c residual marks at the surface indicating flaking can be spotted.

Microstructure changes such as mechanical twins (D at fig. 17c), subgrain formation (E at fig. 17c) and fatigue slip bands (F and G at fig. 18c and 18e, respectively) are observed and attributed to strain accumulation [47]. At applied cyclic strain (F at fig. 18c) higher density of slip bands (of bigger size) than at static strain (G at fig. 18e) can be observed, which is the effect of fatigue influence [47].

Wear track surface becomes more damaged with applied static strain: more abrasive longitudinal marks and marks indicating flaking are noted. Most pronounced flaking is seen at applied cyclic load.

The microstructure is also affected by normal load - higher load leads to higher strain accumulation and the subsurface material undergoes structural changes more intensively. Also the impact on surface is pronounced – surface is smoother at 50 N than at 70 N, there are less scratches and flaking marks as well.

SDSS

Cross-section and wear track surface SEM images of SDSS at 50 N and 70 N normal load are depicted at fig. 19 and fig. 20, respectively.

Similar as at ASS 3-layer structure is observed (fig. 19a), however, the refined nanocrstalline subsurface layer is thinner in case of SDSS for corresponding conditions. In case of 50 N normal load it even appears to be thicker at applied cyclic strain (fig. 19e) than at tribocorrosion conditions (fig. 19a). Though the correlation between no strain and static strain state remains the same as on ASS, meaning at applied static strain the nanocrystalline layer is thinner (higher energy dissipation). Also, fewer defects are observed than on ASS. Subsurface cracks were observed in the nanocrystalline layer (fig. 20a), where the density of defects is highest throughout the material. In the size gradient zone subgrain formation can be spotted (fig. 19e).

For every sample abrasive longitudinal marks and flaking were noted. It appears that at 50 N normal load flaking prevails, whereas at 70 N abrasive marks are more pronounced.

With increasing normal load the number and size of cracks (mainly subsurface) increase (fig. 20a and 20c).

SDSS (50 N normal load)

transversal cross-section **wear surface**

no strain

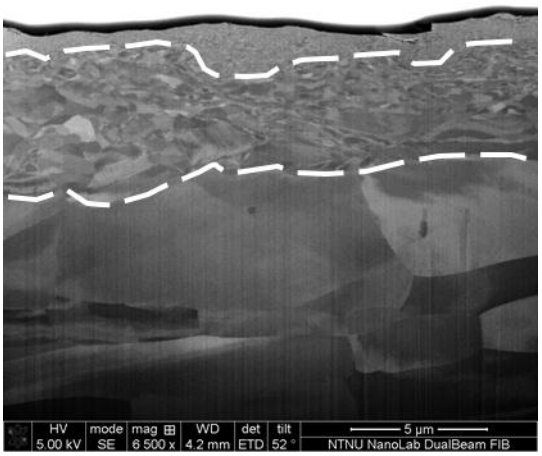

(a)

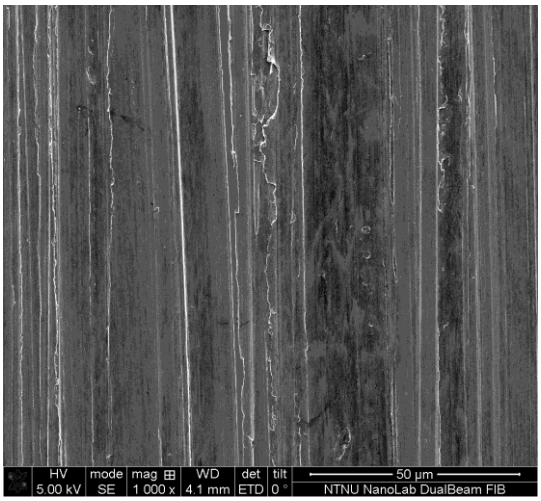

(b)

static strain

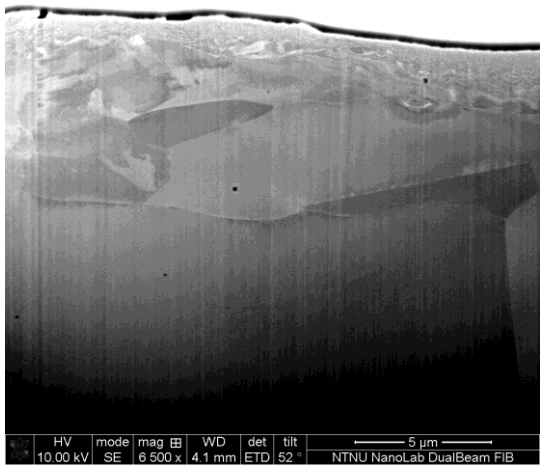

(c)

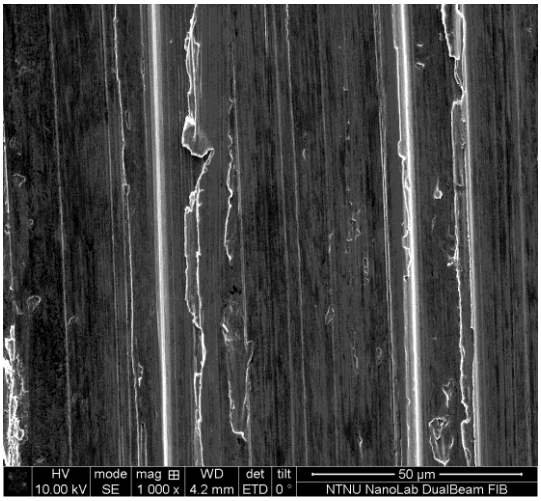

(d)

cyclic strain (1,25 Hz)

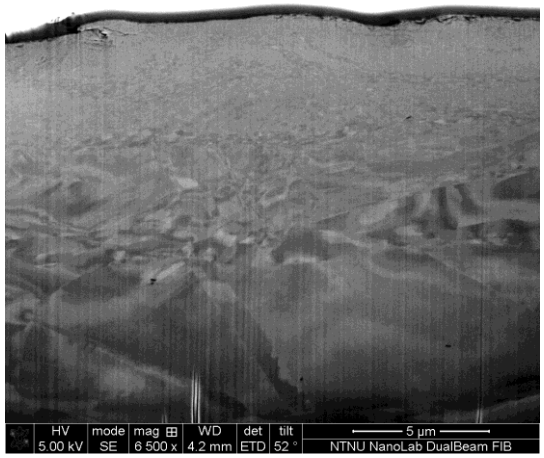

(e)

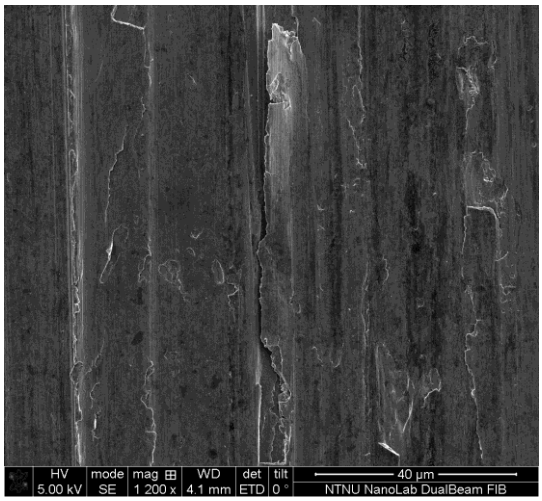

(f)

Fig. 19. SEM images of SDSS wear tracks at 50 N normal load - surface images and transversal cross-sections.

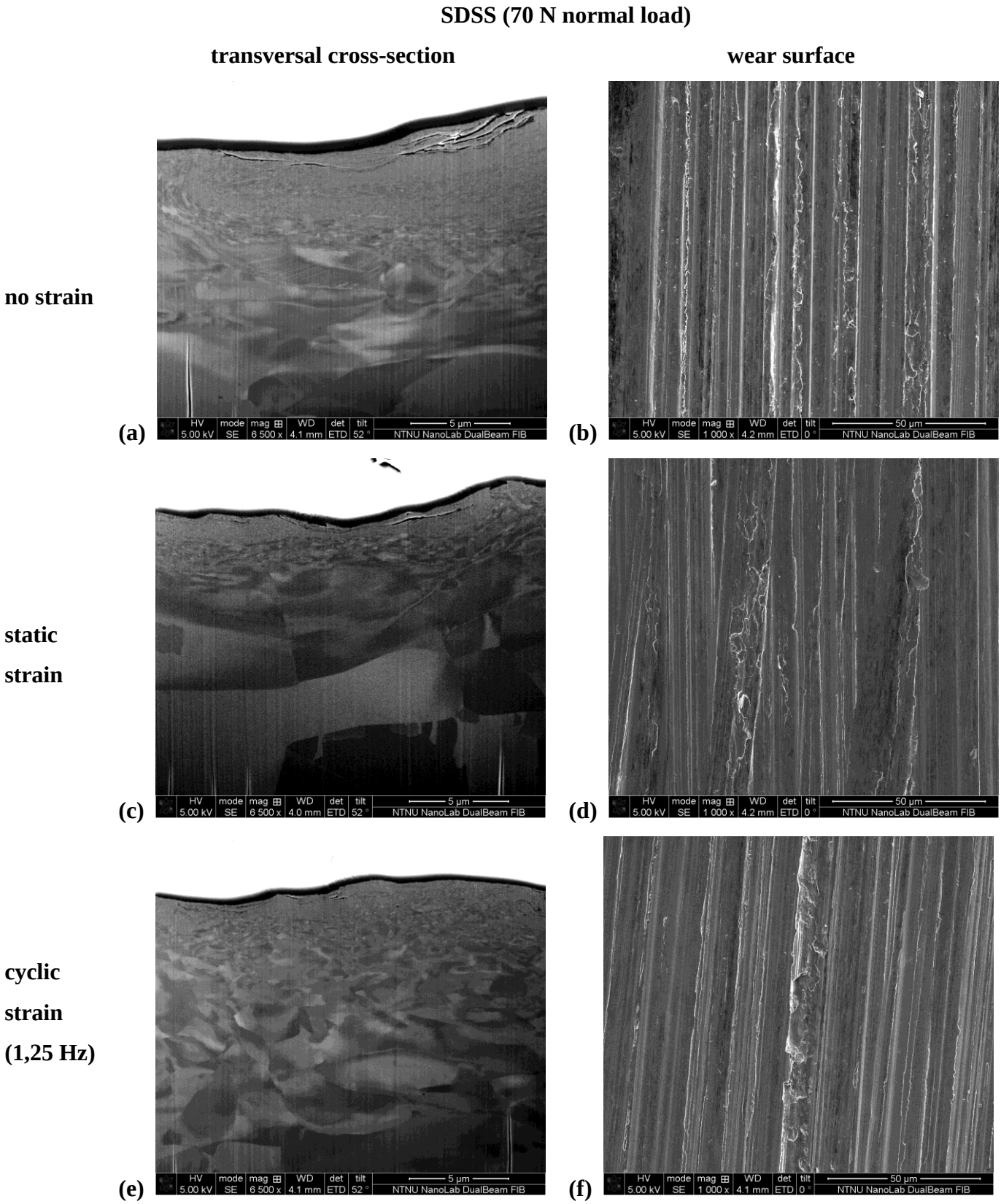

Fig. 20. SEM images of SDSS wear tracks at 70 N normal load - surface images and transversal cross-sections.

4. Discussion

Since very small wear at alumina balls is observed (only adhered metal particles), negligible alumina transfer to the metal surface may be assumed. Surface composition analysis confirmed that approach – no alumina is detected.

Beneath material surface three zones can be distinguished (starting at the surface): mixed nanocrystalline layer (3), plastic deformed layer with grain size gradient (2) and undeformed bulk (3). Zone (2) was observed to exhibit continuous increase of grain size with depth, and suggested to exhibit an exponential decrease in strain [14].

As it was previously shown [37], the passive film thickness is larger inside the wear track than outside - the passive film is thicker than it is reported for this kind of steel (ASS) [55]. This (change of thickness) may be a consequence of mixing or burying of the surface passive film resulting from surface strain [37] and directly affects material properties, such as for example corrosion resistance. Obtained results confirm such approach – surface strain is expected to increase at static loading compared to tribocorrosion exposure and corresponding trend is visible on passive film thickness on both ASS and SDSS (at 50 N). It may also be attributed to surface stresses altering repassivation kinetics [40]. Such a mechanism is reported in [56,57]. It is stated that applied tensile stress increases diffusion rate through the oxide layer, thus facilitates increase of oxide layer thickness.

Passive film is assumed to be responsible for reducing or even blocked annihilation of the dislocations at the surface [37]. Increasing thickness is expected to enhance that effect. It means diffusion of the dislocations into bulk material and consequently higher deformation density favoring dynamic recrystallization reducing grain size. That results in larger subsurface deformed zone.

Grain refinement is also affected by mechanical factors - it may be attributed to large shear strain in the sliding contact [37] (the bigger the applied normal load, the larger the deformed zone). The extent of refinement is also related to the rate of strain accumulation influenced by presence of static/cyclic tensile stresses. In the presence of applied tensile stresses the energy dissipation zone is bigger [40], which confines the extent of refined zone. The mechanical factor (presence of tensile stresses) influences the deformed layer thickness much more than the passive film thickness, based on FIB pictures of ASS and SDSS: fig.17a vs. fig. 17c. and fig. 19a vs. fig. 19c, respectively. Is is observed, that despite thicker passive film the refined layer is much smaller at applied strain compared to tribocorrosion (no strain).

Cyclic loading affects the microstructure to larger extent than static loading. It causes formation of larger deformed zone beneath the surface (fig. 17e vs. fig. 17c), as well as formation of fatigue slip bands (fig. 18e). The explanation is as follows: at applied static bending the material is under stress for the whole test period, whereas at cyclic bending not, because stress is pulsating in the range from 0 to 90% $R_{p0,2}$. Thus, the energy dissipation occurs for shorter period of time compared to static strain, which results in thicker deformed layer.

Multi-degradation processes affect also the electrochemical behavior. At applied static strain an increase in potential drop is observed compared to tribocorrosion (fig. 6 and fig. 8). It can be attributed to bigger metal area exposed to dissolution – at static strain crack initiation can appear. Bigger area also appear with increase in normal load since the ball causes higher surface shear stresses and thus digs deeper into material, which also results in higher potential drop.

There is a direct correlation between passive layer thickness and volume loss, which let us assume that passive layer thickness, besides of corrosion resistance described before, influences the volume loss. The trend is clearly visible on SDSS, to lesser extent on ASS. However it is also assumed to occur on ASS, nevertheless further tests are required to confirm that assumption.

5. Conclusions

1. During multi-degradation two main mechanisms are distinguished:

   a) Tensile stresses affect the surface oxide diffusion rate. Higher diffusion rate facilitates increase of oxide layer thickness, which in turn affects the size of subsurface refined layer and wear volume. During sliding the surface film is broken and de-bounded from the steel substrate. Thicker passive film means bigger debris formation and thus higher volume loss.
   b) Tensile stresses ensure larger energy dissipation zone near the surface, which results in smaller subsurface refined zone. This ‘pure mechanical effect’ of tensile stresses suppresses the ‘chemical effect’ of surface film thickness (factor (a) above), and thus prevails in terms of influencing the subsurface refined layer thickness.

2. Oxide film thickness influences wear volume, material subsurface transformation, corrosion resistance and potential.

6. References

[1] C.B. von der Ohe, Investigating the Multi-degradation Phenomena, Doctoral thesis, Norwegian University of Science and Technology, 2011

[2] C.B. von der Ohe, R. Johnsen, N. Espallargas, Modelling the multi-degradation mechanisms of combined tribocorrosion interacting with statuc and cyclic loaded surfaces of passive metals exposed to seawater, Wear, 269, 607-616

[3] C.B. von der Ohe, R. Johnsen, N. Espallargas, Premature failure of riser tensioner piston rods exposed to offshore splash zone operation – status and review of critical multi-degradation factors, NACE 2009 Paper no.:6125-3934, 2009

[4] C.B. von der Ohe, R. Johnsen, N. Espallargas, Hydraulic cylinders for offshore splash zone operation – a review of piston rod failure cases and alternative concepts, OMAE 2009 Paper no.: OMAE-79039, 2009

[5] D. Kuhlmann-Wilsdorf, The theory of dislocation based crystal plasticity, Phil. Mag. A79 (4) (1999) 955-1008

[6] N. Hansen, D.A. Hughes, Microstructural evolution and hardening parameters, J. Mater Sci. Eng., in press.

[7] X.J. Wang, D.A. Rigney, Sliding behavior of Pb-Sn alloys, Wear 181-183 (1995) 290-301

[8] D.A. Rigney, M.G.S. Maylor, R. Divakar, L.K. Ives, Dislocation structures caused by sliding and by particle impact, Mater Sci. Eng. 81 (1986) 409-425

[9] M. Sato, D.A. Rigney, P.M. Anderson, Rolling-sliding behavior of rail steels, Wear 162-164 (1993) 159-172

[10] D.E. Larsen, The sliding wear of SiC/Aluminum against H-13 tool steel and partially stabilized zirconia, M.S. Thesis, The Ohio State University, 1987

[11] A.T. Alpas, J. Zhang, Effect of SiC particulate reinforcement on the dry sliding wear of aluminium-silicon alloys, Wear 155 (1992) 83-104

[12] Z.Y. Yang, M.G.S. Naylor, D.A. Rigney, Sliding wear of 304 and 310 stainless steels, Wear 105 (1985) 73-86

[13] D. Berthier (Ed.), The third body concept: interpretation of tribological phenomena, in: Proceedings of the 22nd Leeds-Lyon Symposium on Tribology, Elsevier, 1995, in honor of the work of M. Godet

[14] D.A. Rigney, Transfer, mixing and associated chemical and mechanical processes during the sliding of ductile materials, Wear 245 (2000) 1-9

[15] P. Heilmann, J. Don, T.C. Sun, D.A. Rigney, W.A. Glaeser, Sliding wear and transfer, Wear 91 (1983) 131-143

[16] V. Panin, A. Kolubaev, S. Tarasov, V. Popov, Subsurface layer formation during sliding friction, Wear 249 (2002) 860-867

[17] V.L. Popov, A.V. Kolubaev, Analysis of mechanisms for formation of surface layers during friction, Friction Wear 18 (6) (1997) 818-826

[18] V.I. Vladimirov, Problems in friction and wear physics, Wear resistance physics of metallic surfaces, L: FTI RAN, 1988, pp. 8-41

[19] A.F. Joffe, The Physics of crystals, L.B. Loeb, ed., McGraw-Hill Book Co.,Inc.,1928

[20] R. Roscoe, The plastic deformation of cadmium single crystals, Phil. Mag., vol. 21, 1926, pp. 399-406

[21] P.A. Rehbinder, V.I. Likhtman, Effect of surface-active media on strains and rupture in solids, Proceedings of the Second International Congress on Surface Activity, London, no. 3, 1957, pp. 563-580

[22] I.R. Kramer, The effect of surface-active agents on the mechanical behavior of aluminum single crystals, Trans. AIME, vol. 221, no. 5, Oct. 1961, pp. 989-993

[23] J. Ferrante, Exoelectron emission from a clean, annealed magnesium magnesium single crystal during oxygen adsorption, Trans. ASLE, vol. 20, no. 4, Oct. 1976, pp. 328-332

[24] D.H. Buckley, Surface effects in adhesion, friction, wear, and lubrication, Tribology series 5., Elsevier (1981)

[25] G.G. Hancock, H.H. Johnsonm Hydrogen,oxygen and subcritical crack growth in a high strength steel, Trans. AIME, vol. 236, no. 4, Apr. 1966, pp. 513-516

[26] A. Igual Munoz, N. Espallargas, Tribocorrosion mechanisms in sliding contacts, in: D. Landolt, S. Mischler (Eds.), Tribocorrosion of passive metals and coatings, Woodhead Publishing Limited, 2011, pp. 118-152

[27] N. Espallargas, S. Mischler, Tribocorrosion behavior of overlay welded Ni-Cr 625 alloy in sulfuric and nitric acids: Electrochemical and chemical effects, Tribology International, 43, 1209-1217

[28] S. Akonko, D.Y. Li, M. Ziomek-Moroz, Effects of cathodic protection on corrosiove wear of 304 stainless steel, Tribology Letters, 18, 405-410

[29] D. Landolt, S. Mischler, M. Stemp, Electrochemical methods in tribocorrosion: a critical appraisal, Electrochimica Acta, 46, 3913-3929

[30] M. Stemp, M. Mischler, D. Landolt, The effect of mechanical end electrochemical parameters on the tribocorrosion rate of stainless steel in sulphuric acid, Wear, 255, 466-475

[31] Y.N. Kok, N. Akid, P.Eh. Hovsepian, Tribocorrosion testing of stainless steel (SS) and PVD coated SS using a modified scanning reference electrode technique, Wear, 259, 1472-1281

[32] D. Ding, Z. Dai, F. Zhou, G. Zhou, Sliding friction and wear behavior of TC11 in aqueous condition, Wear, 263, 117-124

[33] S. Hassani, K. Raeissi, M. Azzi, D. Li, M.A. Golozar, J.A. Szpunar, Improving the corrosion and tribocorrosion resistance of Ni-Co nanocrystalline coatings in NaOH solution, Corrosion Science, 51, 2371-2379

[34] Y.L. Huang, I.N.A. Oguocha, S. Yannacopoulos, The corrosion wear behavior of selected stainless steels in potash brine, Wear, 258, 1357-1363

[35] J. Stojadinovic, L. Mendia, D. Bouvet, M. Declercq, S. Mischler, Electrochemically controlled wear transitions in the tribocorrosion of ruthenium, Wear, 267, 186-194

[36] I.M. Hutchings, Tribology: Friction and wear of engineering materials, Edward Arnold, London, 1992

[37] J. Perret, E. Boehm-Courjault, M. Cantoni, S. Mischler, A. Beaudouin, W. Chitty, J.P. Vernot, EBSD, SEM and FIB characterization of subsurface deformation during tribocorrosion of stainless steel in sulphuric acid, Wear, 269, 383-393

[38] N. Espallargas, S. Mischler, Dry wear and tribocorrosion mechanisms of pulsed plasma nitrided Ni-Cr alloys, Wear, 270, 464-471

[39] R. Johnsen, C.B. von der Ohe, Tribocorrosion in marine environment, in: D. Landolt, S. Mischler (Eds.), Tribocorrosion of passive metals and coatings, Woodhead Publishing Limited, 2011, pp. 441-474

[40] A. Mitchell, P. Shrotrya, Onset of nanoscale wear of metallic implant materials: Influence of surface residual stresses and contact loads, Wear, 263, 1117-1123

[41] M.Y. He, J.W. Hutchinson, Crack deflection at an interface between dissimilar elastic-materials, Int. J. Solids Struct. 25 (9) (1989) 1053-1067

[42] N. Ye, K. Komvopoulos, Effect of residual stress in surface layer on contact deformation of elastic-plastic layered media, J. Tribol. 125 (2003) 692-699

[43] S. Mischler, S. Debaud, D. Landolt, Wear-accelerated corrosion of passive metals in tribocorrosion systems, J. Electrochem. Soc. 145 (March(3)) (1998)

[44] I. Garcia, D. Drees, J.P. Celis, Corrosion-wear of passivating metals in sliding contacts based on a concept of active wear track area, Wear 249 (2001) 452-460

[45] P. Jemmely, S. Mischler, D. Landolt, Electrochemical modeling of passivation phenomena in tribocorrosion, Wear 237 (2000) 63-76

[46] A. Bronson, J. Nelson, C. Kang, Analysis of the scribing technique for determining the corrosive wear of an Fe-21 wt.%Cr-19 wt.%Ni alloy, Wear 154 (1992) 387-401

[47] C.B. von der Ohe, R. Johnsen, N. Espallargas, Multi-degradation behavior of austenitic and super duplex stainless steel – The effect of 4-point static and cyclic bending applied to a simulated seawater tribocorrosion system, Wear, 288, 39-53

[48] C. B. von der Ohe, R. Johnsen, N. Espallargas, A multi-degradation test rig for studying the synergy effects of tribocorrosion interracting with 4-point static and cyclic bending, Wear, 271 (2011), 2978-2990

[49] UNS S31603 Material Certificate Number; 2008SK0042618, Heat No.: 827061

[50] UNS S32750 Material Certificate Number, 7083936.R00, Heat No.: 472324

[51] http://www.jotun.com/Datasheets/Download?url=%2FTDS%2FTDS__16560__Jotamastic+90__Euk__GB.pdf

[52] K. Hashimoto, K. Asami, K. Teramoto, An X-ray photo-electron spectroscopic study on the role of molybdenum in increasing the corrosion resistance of ferritic stainless steels in HCl, Corrosion Science, 19 (1979), pp. 3-14

[53] K. Sugimoto, Y. Sadawa, The role of molybdenum additions to austenitic stainless steels in the inhibition of pitting in acid chloride solutions, Corrosion Science, 17 (1977), pp. 425-445

[54] Claes-Olof A. Olsson, The influence of nitrogen and molybdenum on passive films formed on the austeno-ferritic stainless steel 2205 studied by AES and XPS, Corrosion Science, 37 (1995), pp. 467-479

[55] D. Landolt, Corrosion and Surface Chemistry of Metals, EPFL Press/CRC, 2007

[56] V. Vignal, R. Oltra, M. Verneau, L. Coudreuse, Influence of an elastic stress on the conductivity of passive films, Mater. Sci. Eng. A. 303 (2001) 173–178

[57] D. Sidane a, O. Devos a, M. Puiggali a, M. Touzet a, B. Tribollet b, V. Vivier, Electrochemical characterization of a mechanically stressed passive layer, Electrochemistry Communications, 13 (2011), 1361–1364

[58] D.A. Shirley, High-resolution x-ray photoemission spectrum of the valence bands of gold, Phys. Rev. B. 5 (1972) 4709–4714

APPENDIX A – Risk assessment

NTNU	Risikovurdering	Utarbeidet av	Nummer	Dato
HMS		HMS-avd.	HMSRV2601	22.03.2011
		Godkjent av		Erstatter
		Rektor		01.12.2006

Enhet: NTNU, Institutt for produktutvikling og materialer **Dato: 13.02.2015**

Linjeleder:

Deltakere ved kartleggingen *(m/ funksjon)*: **Maciej Andrzejewski** (student), **Nuria Espallargas** (veileder), **Amin Hossein Zavieh** (medveileder)

(Ansv. veileder, student, evt. medveiledere, evt. andre m. kompetanse)

Risikovurderingen gjelder hovedaktivitet: Masteroppgave student: **Maciej Andrzejewski**. Tittel på oppgaven: **Multidegradation processes in Direct Riser Tensioning (DRT) systems for O&G.**

Signaturer: *Ansvarlig veileder:* Nuria Espallargas *Student:* Maciej Andrzejewski

ID nr	Aktivitet fra kartleggings-skjemaet	Mulig uønsket hendelse/ belastning	Vurdering av sannsyn-lighet	Vurdering av konsekvens:				Risiko-Verdi (menn-eske)	Kommentarer/status Forslag til tiltak
			(1-5)	Menneske (A-E)	Ytre miljø (A-E)	Øk/ materiell (A-E)	Om-dømme (A-E)		
1	Clearing the samples/alumina balls	Contact of the chemicals (ethanol, acetone) with eyes or respiratory system	3	A	A	A	A	A3	
2	Grinding/polishing the samples	Scratches	2	A	A	A	A	A2	
3	Preparing/performing a test	Scratches	3	A	A	A	A	A3	
4	Fitting protective caps on both ends of a sample	Burns	2	A	A	A	A	A2	
5	Ussing supporting devices (computer, microscopes, ultrasonic cleaner)	Electric shock	3	B	A	A	C	A3	

NTNU HMS	Risikovurdering	Utarbeidet av	Nummer	Dato
		HMS-avd.	HMSRV2601	22.03.2011
		Godkjent av		Erstatter
		Rektor		01.12.2006

Enhet: NTNU, Institutt for produktutvikling og materialer **Dato: 13.02.2015**

Linjeleder:

Deltakere ved kartleggingen (m/ funksjon)**: Maciej Andrzejewski** (student), **Nuria Espallargas** (veileder)**, Amin Hossein Zavieh** (medveileder)
(Ansv. veileder, student, evt. medveiledere, evt. andre m. kompetanse)

Kort beskrivelse av hovedaktivitet/hovedprosess: Masteroppgave student: **Maciej Andrzejewski**. Tittel på oppgaven: **Multidegradation processes in Direct Riser Tensioning (DRT) systems for O&G.**

Er oppgaven rent teoretisk? (JA/NEI)**: NEI** *«JA» betyr at veileder innestår for at oppgaven ikke inneholder noen aktiviteter som krever risikovurdering. Dersom «JA»: Beskriv kort aktiviteteten i kartleggingskjemaet under. Risikovurdering trenger ikke å fylles ut.*

Signaturer: *Ansvarlig veileder:* Nuria Espallargas *Student:* Maciej Andrzejewski

ID nr.	Aktivitet/prosess	Ansvarlig	Eksisterende dokumentasjon	Eksisterende sikringstiltak	Lov, forskrift o.l.	Kommentar
1	Cleaning the samples/alumina balls	Maciej Andrzejewski		Protective glasses and gloves		Possible contact of the chemicals (ethanol, acetone) with eyes or respiratory system
2	Grinding/polishing the samples	Maciej Andrzejewski		Protective glasses and gloves, hearing protector		Possible scratches; grinding the edges of the samples (grinding machine); polishing samples' surface (manually)
3	Preparing/performing a test	Maciej Andrzejewski		Protective glasses and gloves		Possible scratches and bruises during assembling the test rig/a sample and during machine operation
4	Fitting protective caps on both ends of a sample	Maciej Andrzejewski		Protective glasses and gloves		Possible burns
5	Ussing supporting devices (computer, microscopes, ultrasonic cleaner)	Maciej Andrzejewski				Possible electric shock

NTNU HMS/KS	Risikomatrise	utarbeidet av	Nummer	Dato
		HMS-avd.	HMSRV2604	08.03.2010
		godkjent av		Erstatter
		Rektor		09.02.2010

MATRISE FOR RISIKOVURDERINGER ved NTNU

KONSEKVENS						
	Svært alvorlig	E1	E2	E3	E4	E5
	Alvorlig	D1	D2	D3	D4	D5
	Moderat	C1	C2	C3	C4	C5
	Liten	B1	B2	B3	B4	B5
	Svært liten	A1	A2	A3	A4	A5
		Svært liten	Liten	Middels	Stor	Svært stor
		SANNSYNLIGHET				

Prinsipp over akseptkriterium. Forklaring av fargene som er brukt i risikomatrisen.

Farge	Beskrivelse
Rød	Uakseptabel risiko. Tiltak skal gjennomføres for å redusere risikoen.
Gul	Vurderingsområde. Tiltak skal vurderes.
Grønn	Akseptabel risiko. Tiltak kan vurderes ut fra andre hensyn.

NTNU HMS	Risikovurdering	Utarbeidet av	Nummer	Dato
		HMS-avd.	HMSRV2601	22.03.2011
		Godkjent av		Erstatter
		Rektor		01.12.2006

Sannsynlighet vurderes etter følgende kriterier:

Svært liten 1	Liten 2	Middels 3	Stor 4	Svært stor 5
1 gang pr 50 år eller sjeldnere	1 gang pr 10 år eller sjeldnere	1 gang pr år eller sjeldnere	1 gang pr måned eller sjeldnere	Skjer ukentlig

Konsekvens vurderes etter følgende kriterier:

Gradering	Menneske	Ytre miljø Vann, jord og luft	Øk/materiell	Omdømme
E Svært Alvorlig	Død	Svært langvarig og ikke reversibel skade	Drifts- eller aktivitetsstans >1 år.	Troverdighet og respekt betydelig og varig svekket
D Alvorlig	Alvorlig personskade. Mulig uførhet.	Langvarig skade. Lang restitusjonstid	Driftsstans > ½ år Aktivitetsstans i opp til 1 år	Troverdighet og respekt betydelig svekket
C Moderat	Alvorlig personskade.	Mindre skade og lang restitusjonstid	Drifts- eller aktivitetsstans < 1 mnd	Troverdighet og respekt svekket
B Liten	Skade som krever medisinsk behandling	Mindre skade og kort restitusjonstid	Drifts- eller aktivitetsstans < 1uke	Negativ påvirkning på troverdighet og respekt
A Svært liten	Skade som krever førstehjelp	Ubetydelig skade og kort restitusjonstid	Drifts- eller aktivitetsstans < 1dag	Liten påvirkning på troverdighet og respekt

Risikoverdi = Sannsynlighet x Konsekvens
Beregn risikoverdi for Menneske. Enheten vurderer selv om de i tillegg vil beregne risikoverdi for Ytre miljø, Økonomi/materiell og Omdømme. I så fall beregnes disse hver for seg.

Til kolonnen "Kommentarer/status, forslag til forebyggende og korrigerende tiltak":
Tiltak kan påvirke både sannsynlighet og konsekvens. Prioriter tiltak som kan forhindre at hendelsen inntreffer, dvs. sannsynlighetsreduserende tiltak foran skjerpet beredskap, dvs. konsekvensreduserende tiltak.